Mineral UV filters and their effects on Pocillopora damicornis metabolome

Claire Guillier, Maeva Giraudo, Fanny Clergeaud, Evane Thorel, Leïla Chapron, Lionel Marcon, Philippe Lebaron, Emeline Houël, Didier Stien

▶ **To cite this version:**

Claire Guillier, Maeva Giraudo, Fanny Clergeaud, Evane Thorel, Leïla Chapron, et al.. Mineral UV filters and their effects on Pocillopora damicornis metabolome. Science of the Total Environment, 2025, 991, pp.179961. ⟨10.1016/j.scitotenv.2025.179961⟩. ⟨hal-05133154⟩

HAL Id: hal-05133154

https://hal.science/hal-05133154v1

Submitted on 27 Jun 2025

HAL is a multi-disciplinary open access archive for the deposit and dissemination of scientific research documents, whether they are published or not. The documents may come from teaching and research institutions in France or abroad, or from public or private research centers.

L'archive ouverte pluridisciplinaire **HAL**, est destinée au dépôt et à la diffusion de documents scientifiques de niveau recherche, publiés ou non, émanant des établissements d'enseignement et de recherche français ou étrangers, des laboratoires publics ou privés.

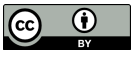

Distributed under a Creative Commons CC BY 4.0 - Attribution - International License

Mineral UV filters and their effects on *Pocillopora damicornis* metabolome

Claire Guillier[a], Maeva Giraudo[a], Fanny Clergeaud[a], Evane Thorel[a], Leïla Chapron[b], Lionel Marcon[a], Philippe Lebaron[a], Emeline Houël[a], Didier Stien[a,*]

[a] Sorbonne Université, Université de Perpignan Via Domitia, CNRS, Laboratoire de Biodiversité et Biotechnologies Microbiennes, LBBM, F-66650 Banyuls-sur-Mer, France.

[b] Sorbonne Université, CNRS, Laboratoire d'Ecogéochimie des Environnements Benthiques, LECOB, F-66650 Banyuls-sur-Mer, France.

* Corresponding author: didier.stien@cnrs.fr, Tel.: +33 4 30 19 24 76

Abstract

The rising use of sunscreens and cosmetics containing ultraviolet (UV) filters has increased their presence in marine ecosystems. UV filters encompass a wide range of organic and mineral compounds with diverse behaviors and properties in aquatic environments. The mineral filters titanium dioxide (TiO_2) and zinc oxide (ZnO) are commonly found in cosmetic products as particles or nanoparticles (NPs) and are increasingly used as alternatives to organic UV filters. In this study, the effects of a coated form of TiO_2 (Solaveil^{TM} XTP_1, 60 nm, hydrophobic) and uncoated ZnO particles from two different sizes (Zano$^{®}$10 and Zano$^{®}$M, 60 and 250 nm, hydrophilic) were assessed on the symbiotic tropical coral *Pocillopora damicornis* using an untargeted metabolomic approach. Corals were exposed for seven days to environmentally relevant particle concentrations (5 to 1000 µg.L^{-1}), and their metabolomes were analyzed using UHPLC-HRMS/MS. While TiO_2 exposure did not induce significant metabolomic changes, both sizes of ZnO particles caused shifts in the metabolome of the coral's symbiotic dinoflagellates, leading to a noticeable decrease in the relative concentrations of symbiont lipids and pigments. A size-dependent toxicity of ZnO was observed: ZnO NPs triggered signs of bleaching at concentrations as low as 300 µg.L^{-1}, whereas larger ZnO particles exhibited only mild effects at the highest concentration tested (1000 µg.L^{-1}). This underscores the critical role of

ATR: Attenuated Total Reflection; BP-3: Oxybenzone; CD: Compound Discoverer^{TM}; DGCC: 1,2-Diacylglyceryl-3-*O*-carboxy-(hydroxymethyl)-choline; DGDG: Digalactosyldiacylglycerol; DMSO: Dimethyl sulfoxide; DNP: Dictionary of Natural Products; EHMC: Octinoxate; FASW: Filtered Artificial Sea Water; FDR: False discovery rate; FTIR: Fourier Transform InfraRed spectroscopy; GNPS: Global Natural Products Social Molecular Networking; GSL: Glycosphingolipid; LDGCC: Lyso-diacylglycerylcarboxy-hydroxymethylcholine; Log_2 FC: Log_2(fold-change); LPC: Lyso-phosphatidylcholine; MGDG: Monogalactosyldiacylglycerol; MoNa: MassBank of North America; NP: Nanoparticle; OC: Octocrylene; PEG: Polyethylene glycol; PSII: Photosystem II; PRM: Parallel Reaction Monitoring; ROS : Reactive Oxygen Species; SEM: Scanning electron microscopy; TEM: Transmission electron microscopy; TiO_2: Titanium Dioxide; UV: Ultraviolet; ZnO: Zinc Oxide; ZP: Zeta Potential

particle size in determining toxicity. This research highlights the contrasting effects of different mineral UV filters on symbiotic corals and aims to inform cosmetic companies in selecting mineral filters that minimize harmful impacts on coral reefs.

Keywords: coral bleaching, metabolomics, inorganic sunscreen, nanoparticles, Symbiodiniaceae

1. Introduction

Over recent decades, coral reefs have experienced a persistent decline, characterized by frequent and severe bleaching events (Suggett and Smith, 2020). Coral bleaching occurs when the symbiotic relationship between corals and their endosymbiotic dinoflagellates, commonly referred to zooxanthellae (*Symbiodinium* spp.), breaks down (Nielsen et al., 2018). This disruption leads to pigment degradation and/or the loss of zooxanthellae, which can ultimately result in coral mortality (Bridge et al., 2014). Together with the coral host and its associated microbiota, these symbionts form the coral holobiont — a complex symbiotic system whose stability is crucial for reef health and resilience (Berkelmans and Van Oppen, 2006). The integrity of this symbiotic relationship is increasingly threatened by global climate change, which alters sea temperatures and ocean acidity (Cameron et al., 2022), as well as by localized stressors, including the influx of sunscreen-derived chemicals into coastal waters (Tovar-Sánchez et al., 2013). While sunscreens play a critical role in protecting human health from the adverse effects of ultraviolet (UV) radiations, their widespread use driven by rising tourism, has led to the accumulation of UV filters in marine ecosystems, raising concerns about their impact on aquatic organisms (Sánchez-Quiles and Tovar-Sánchez, 2015). Among these UV filters, certain organic compounds such as benzophenone-3 (or oxybenzone, BP-3), ethylhexyl methoxycinnamate (or octinoxate, EM), and octocrylene (OC), have received particular attention due to their adverse effects on marine organisms, especially coral (ANSES, 2022). Several studies have demonstrated that BP-3 and EM can disrupt the coral microbiome equilibrium, induce coral bleaching and promote viral proliferation, potentially leading to coral death (Conway et al., 2021; Danovaro et al., 2008; Yang et al., 2023). OC has been shown to accumulate in coral tissues, both in its initial form and as derivatives, and trigger deleterious processes such as oxidative stress and mitochondrial dysfunction (He et al., 2019; Stien et al., 2019; Thorel et al., 2022; Tsui et al.,

2017). In response to these findings, several countries have implemented strict regulations or outright bans on sun care products containing these three UV filters. For example, OC has been banned in Palau (2018), the Marshall Islands (2019), and the Virgin Islands (2020). Similarly, both EM and BP-3 have been banned in Key West (2019), Thailand (2021) and Hawaii (2021), reflecting a growing international commitment to protect marine ecosystems from sunscreen pollution. Consequently, sun care formulations are undergoing significant reformulation to meet both human health standards and environmental sustainability goals.

This shift has led to the increased adoption of mineral UV filters, primarily titanium dioxide (TiO_2) and zinc oxide (ZnO), as alternatives to organic UV filters in many sun care products (Schneider and Lim, 2019). These mineral filters are often incorporated in the form of nanoparticles (NPs), whose UV-protected efficiency is closely tied to their physicochemical characteristics, including particle size, shape, surface charge and surface coatings. These features enhance formulation stability and broaden UV protection compared to their organic counterparts (Smijs and Pavel, 2011). In this context, there is growing interest in understanding the fate and behavior of mineral UV filters once released into aquatic environments. However, limited quantitative data exist on their environmental concentrations largely due to the difficulty in distinguishing anthropogenic inputs from natural particulate matter. Some measurements from Mediterranean coastal areas have been reported: Tovar-Sánchez et al. (2013) found TiO_2 concentrations ranging from 12-37 $\mu g.L^{-1}$ and ZnO from 0.8-10.8 $\mu g.L^{-1}$ in surface waters off the coast of Majorca, while organic filters were detected at concentrations in the $ng.L^{-1}$ range. Similarly, Thallinger et al. (2023) reported higher TiO_2 levels compared to organic filters, with concentrations between 20-296 $\mu g.L^{-1}$ in Palavas-les-Flots, France. In Marseille, Labille et al. (2020) observed TiO_2 concentrations of 100-900 $\mu g.L^{-1}$ and ZnO levels between 20-50 $\mu g.L^{-1}$ in surface water, with lower values of 10-15 $\mu g.L^{-1}$ and 1-3 $\mu g.L^{-1}$, respectively, detected in deeper water layers.

The distribution, persistence and bioavailability of mineral UV filters are governed by their intrinsic properties (Mitjans et al., 2023; Samei et al., 2019; Yung et al., 2017), as well as by environmental parameters such as temperature, pH, salinity, and UV radiation (Lewicka et al., 2011; Pagnout et al., 2012; Li et al., 2013). These factors ultimately influence particle-organism interactions and associated

toxicity mechanisms. The size-dependent toxicity of metal oxide particles, such as TiO_2 and ZnO, has been documented in various aquatic species. Nano-sized dispersed TiO_2 and ZnO have been shown stronger inhibitory effects on algal growth (e.g., *Nitzschia closterium* and *Dunaliella tertiolecta)* compared to their bulk counterparts (Manzo et al., 2013; Xia et al., 2015). In aquatic invertebrates such as *Daphnia magna*, smaller TiO_2 and ZnO agglomerates accumulate more readily in the digestive tract (Kim et al., 2010; Lopes et al., 2014). In *Danio rerio*, TiO_2 NPs at 50 $mg.L^{-1}$ induced significant gill cell damage over 96 hours, whereas bulk TiO_2 caused negligible effects (Xiong et al., 2011).

By contrast, the role of surface coatings in modulating toxicity remains underexplored. These coatings — either mineral (e.g., Al_2O_3 or SiO_2) or organic (e.g., stearic acid, silane, polyacrylic acid) — affect particle properties such as wettability, dispersion, and texture, facilitating their integration into formulations by altering their hydrophobicity/hydrophilicity (Slomberg et al., 2021). Coatings may also enhance particles stability by reducing undesired photocatalytic reactions, which may also promote their persistence into the environment after release (Mbanga et al., 2022; Thallinger et al., 2023). While coatings may mitigate toxicity by altering aggregation, solubility or dispersion in water (Lai et al., 2021; Yung et al., 2017), they can also influence particle uptake and depuration in aquatic organisms (Connolly et al., 2022; Lai et al., 2021).

The impact of inorganic UV filters on corals remains insufficiently understood. However, emerging evidence suggests that these filters may contribute to coral bleaching through symbiont loss and reduced photosynthetic efficiency (Fel et al., 2019; Jovanović and Guzmán, 2014), as well as by promoting microbial enrichment following ZnO exposure (Corinaldesi et al., 2018). Still, many of these studies lack detailed physicochemical characterization of the NPs used, which is essential for accurately assessing their toxicity and ensuring comparability between studies. Based on previous studies focusing on corals, it can be hypothesized that ZnO particles will exhibit greater toxicity than TiO_2 particles due to their higher solubility and potential for Zn^{2+} release. Additionally, nanoparticles are expected to cause more pronounced biological effects compared to larger particles of the same composition, as smaller particles have higher surface area-to-volume ratios and typically higher dissolution rates. To overcome such limitations, metabolomics has emerged as a promising and integrative approach for exploring stress responses in complex biological systems such as the coral

holobiont. While primarily used to investigate stress-specific responses to coral bleaching (Pei et al., 2022; Roach et al., 2021; Sogin et al., 2016), metabolomics has also proven valuable in evaluating the effects of organic UV filters (Clergeaud et al., 2023; Stien et al., 2020). By analyzing the complete set of metabolites in an organism, untargeted metabolomics can detect subtle, early biochemical changes induced by nanoparticle exposure, providing light on toxicity mechanisms at a molecular level.

The present study aims to further elucidate the effects of TiO_2 and ZnO particles and NPs on the symbiotic tropical scleratinian coral *Pocillopora damicornis*. This ubiquitous Indo-Pacific species thrives in shallow waters (Bramanti et al., 2015). As a fast-growing, reef building (hermatypic) coral, *Pocillopora damicornis* plays a fundamental ecological role by facilitating the settlement of various other species, making it an ideal model for assessing risks to coral reef ecosystems (Brener-Raffalli et al., 2018). In this study, corals were exposed to increasing concentrations (5, 50, 300 and 1000 $\mu g.L^{-1}$) of one stearic acid-alumina coated TiO_2 (Solaveil^{TM} XTP_1) and two ZnO nanopowders of different sizes (Zano10$^{®}$ and ZanoM$^{®}$) to evaluate metabolomic shifts associated with stress induced by these widely used mineral UV filters.

2. Materials and Methods

2.1. Mineral UV filters characterization

2.1.1 Mineral UV filters

Solaveil^{TM} XTP_1 alumina stearic acid coated nanoparticles (TiO_2 NPs) were purchased from Croda (Croda Personal Care, Montigny-le-Bretonneux, France). Zano$^{®}$10 and Zano$^{®}$M (EverCare, Netherlands, Eijsden) uncoated zinc oxide particles (ZnO) were purchased from Comercial Química Massó (Barcelona, Spain). Particles specific surface area given by the supplier for Zano$^{®}$10 and Zano$^{®}$M are respectively of 29.1 m^2/g and 9 m^2/g (BET technical measurements), and not available for Solaveil^{TM} XTP_1. Purity of each mineral UV filter tested is greater than 98% according to the data provided by suppliers.

2.1.2 Fourier transform infrared spectrometry analysis (FTIR)

The aim of FTIR analysis was to confirm the presence or absence of surface coatings on the mineral UV filters and to identify characteristic functional groups that may influence their environmental

behavior and interaction with biological systems. The analysis was performed on the pristine powder form of each sample (Solaveil™ XTP1, Zano®10, and Zano®M), without any pre-treatment, in order to assess their chemical surface composition as supplied by the manufacturer.

All spectra were recorded using a handheld Fourier transform infrared (FTIR) spectrometer (Agilent 4300, Agilent Technologies, USA) equipped with a single-reflection attenuated total reflectance (ATR) sensor. Measurements were conducted in the wavenumber range of 4000–400 cm^{-1} with a resolution of 4 cm^{-1}, and 68 scans were averaged per spectrum. This method allows for non-destructive analysis of surface-bound organic or inorganic moieties, such as stearate or carboxylate groups, potentially indicative of surface coatings or synthesis residues.

2.2.2. Transmission Electron Microscopy (TEM)

Transmission electron microscopy (TEM, S-3400N, HITACHI, Japan) was used to assess the morphology and size range of Solaveil™ XTP_1, Zano®10 and Zano®M primary particles. To do so, a brush was dipped into UV filters powders, and the particles were sprayed over a glow-discharged copper grid. The primary particle size distribution was pictured under an operating voltage set at 80 kV and determined by measuring the length of approximately 300 particles, by a manual point-to-point measurement on AMT software (512 version 5.42.544 Q, USA).

2.2.3 Scanning Electron microscope (*SEM*)

Similar to TEM sample preparation, a few micrograms of particles were sprayed onto carbon tape attached to an aluminum support for scanning electron microscopy (SEM, JSM-IT800 SHL LV, Jeol, Japan). Particle images were collected at a working distance of 4 mm, with an accelerating voltage set at 2 kV for Solaveil™ XTP_1 and Zano®10, and 5 kV for Zano®M.

2.2.4. Zeta potential and hydrodynamic size measurements

Electrophoretic mobility and hydrodynamic diameters of TiO_2 and ZnO particles were measured using a Malvern Zetasizer® Nano-ZS instrument based on Dynamic Light Scattering (DLS). Measurements were performed at 25 °C on 1 $mg \cdot L^{-1}$ suspensions prepared in filtered artificial seawater (FASW), using the same dispersion protocols as for coral exposures. Hydrophobic particles (e.g., Solaveil™ XTP1) were first dispersed in a DMSO solution containing 0.1% Emulium® Illustro,

then diluted 1:1000 in FASW. All suspensions were sonicated (10–30 min) and vortexed prior to measurement.

Each sample was measured in triplicate (8 runs per measurement), and the cuvettes were re-agitated between runs to prevent sedimentation. Hydrodynamic diameters were determined using the Mie theory algorithm provided by the instrument software. For each particle type, we report volume-weighted mean diameters, considered more representative for polydisperse samples, and additionally include intensity-weighted diameters and polydispersity indices (PDI) in the supplementary material (Table Sx). The residuals of curve fitting were within acceptable limits, and measurement quality was validated by the analytical platform.

Zeta potential (ZP) measurements yielded values between -6.3 and -9.6 mV for particle suspensions, similar to the background of the FASW control (-6 mV), indicating low electrostatic repulsion and a tendency to form aggregates."

2.3. Rearing of *Pocillopora damicornis*

Colonies of *P. damicornis* were maintained at the Banyuls Observatory nursery since their collection from Oman in 2014 (CITES permit 37/2014). They are cultured in FASW (salinity = 36 $g.L^{-1}$, pH = 8, and temperature maintained at 24 ± 1 °C) prepared using reverse osmosis-purified water mixed with TropicMarin™ Salt (Tropic Marin PRO REEF salt, Wartenberg, Germany). The lighting is provided by Ecotech Marine Radion G5 lamps (model XR15 Pro, Bethlehem, PA, USA), set to deliver a photosynthetic photon flux density of 250 $\mu mol.m^{-2}.s^{-1}$ under a 10:14-hour light:dark photoperiod. Prior exposure, small coral fragments (about 5 cm) were cut from a mother colony and suspended to a fishing line (nylon) for a one-month acclimation period to ensure a complete tissue repair. Colonies and suspended fragments were fed daily with brine shrimps *Artemia salina* (approximatively 800 shrimps per liter in culture tank).

2.4. Exposure to Zano®10, Zano®M and Solaveil™ XTP_1

The concentrations of the tested suspensions were defined on the basis of a preliminary acute toxicity test and were set at 1000 $\mu g.L^{-1}$ for Solaveil™ XTP_1 and 5, 50, 300 and 1000 $\mu g.L^{-1}$ for Zano®10 and Zano®M. Stock suspensions of Zano®10 and Zano®M were prepared at concentrations of 5, 50, 300

and 1000 mg.L^{-1} in MilliQ water. For each exposure condition, 200 µL of the stock suspension was dispersed into beakers containing 200 mL of FASW freshly collected from the culture aquarium to achieve the nominal concentrations of 5, 50, 300 and 1000 µg.L^{-1} of Zano®10 and Zano®M suspensions. Due to the insolubility of Solaveil™ XTP_1 in water, solutions were prepared in DMSO containing 0.1% emulsifier (Emulium® Illustro, Gattefossé, Saint-Priest, France).

Each coral nubbin was immersed in individual exposure beakers (N = 5 per condition) and exposed for seven days. Unexposed controls were placed in 200 mL of FASW only, while solvent controls (DMSO+0.1% emulsifier) were used for Solaveil™ XTP_1 exposure. These solvent controls were subjected to the same metabolomic analysis as the test conditions and showed no significant differences from FASW controls (data not shown). The exposure medium was renewed daily, maintaining identical physicochemical parameters than acclimation period (salinity = 36 g.L^{-1}; pH = 8; temperature = 24 ± 1 °C), oxygen saturation was maintained by gentle air flux, and the lighting conditions were kept identical to those in coral nurseries. Daily photographs of the coral pieces were taken at a consistent time to monitor polyps retraction (SI, figures S1 – S5). Corals were not fed during the exposure.

2.5. Extraction and metabolomic profiling

Metabolome extraction was performed at the end of the seven days of exposure as described previously (Thorel et al., 2022). Briefly, after methanol/acetonitrile 1:1 extraction, extracts (1 mg.mL^{-1}, 2 µL injection in column) were analyzed using an Ultimate 3000™ UHPLC system (Thermo Fisher Scientific, Waltham, MA, USA) coupled to an Orbitrap MS/MS FT Q-Exactive focus mass spectrometer as previously described (Stien et al, 2019). Parallel Reaction Monitoring **(**PRM) analyses were conducted to obtain missing MS/MS data. Retention times were checked before targeted analyses. The resolution was 35.000, AGC target 5.10^4, isolation window 0.4 Da, and stepped normalized collision energy 15/30/45 was used with 15 s dynamic exclusion. Blank injections were performed to remove irrelevant chemical background. The retention time window was set to 2–17 min. The maximum shift for alignment was 0.1 min, the maximum mass tolerance was 2 ppm, and the minimum peak intensity was 2.10^6. For Zano®10 differential analysis, only 4 replicates were used due to a strong polyethylene glycol (PEG) derivative contamination of one of the replicates (Zano®10, 50

230 µg.L^{-1}), confirmed by comparison to a commercial standard (Polyoxyethylene glycol (10) tridecyl
231 ether, CAS: 78330-21-9, Sigma-Aldrich). Annotation was carried out by assessing molecular formulas
232 accurately calculated on the basis of high-resolution mass spectrometry (Freestyle software 1.5,
233 Thermo Fisher Scientific) and comparing them to databases (Dictionary of Natural Products – DNP
234 (CHEMnetBASE, Taylor&Francis, Informa, London, UK), LipidMaps (https://www.lipidmaps.org/),
235 LOTUS (https://lotus.naturalproducts.net/) and SciFinder^{n} (American Chemical Society)) to offer
236 candidate compounds. MS/MS spectra were then submitted to databases for comparison (Global
237 Natural Products Social Molecular Networking – GNPS (https://gnps.ucsd.edu) (Wang et al., 2016),
238 MassBank of North America – MoNa (https://mona.fiehnlab.ucdavis.edu), and SIRIUS software (5.8.3
239 version, Lehrstuhl Bioinformatik, Jena), (Dührkop et al., 2019) or manually elucidated with
240 fragmentation pattern and structural similarities. For annotation, standards L-tryptophan (CAS: 73-22-
241 3), β-sitosterol (CAS: 83-46-5) and β-carotene (CAS: 7235-40-7) were acquired from Sigma-Aldrich,
242 and injected as 5 µg.mL^{-1} methanolic solutions in the same conditions for comparison of retention time
243 and MS/MS spectra.
244
245 **2.6 Statistical analysis**
246 Data processing and visualization were performed using Compound Discoverer™ software (CD 2.1,
247 ThermoFisher, Villebon, France). The relative concentrations of ions in exposed groups were
248 compared to those in control groups (as FASW condition for Zano®10 and Zano®M, and DMSO +
249 0.1% emulsifier condition for Solaveil™ XTP_1) at each tested concentration to calculate Log_2(fold
250 change) (Log_2(FC)). For Solaveil™ XTP_1, *p*-values for differences in relative ion concentrations were
251 determined using a t-test. For Zano®10 and Zano®M, *p*-values were determined using analysis of
252 variance (ANOVA) followed by Tukey's HSD post hoc test. Ions with a Log_2 (FC) > ±1 and p-value <
253 0.05 were initially flagged as candidates for annotation. Each selected feature was then manually
254 inspected for signal quality, annotation confidence, and consistency across replicates. This expert-
255 based approach prioritizes biologically coherent patterns across related metabolites (e.g., carotenoids,
256 lipids), which we find more robust than relying solely on statistical corrections.
257
258 **3. Results**

3.1 Mineral UV filters characterization

FTIR analysis of Solaveil™ XTP_1 revealed a broad peak centered around 3400 cm^{-1}, attributed to hydroxyl groups present on the alumina surface (Figure 1). Strong peaks observed at 2853 and 2920 cm^{-1} correspond to the symmetric and asymmetric vibrations of CH_2 groups (Ahmad et al., 2021; Feng et al., 2018). Intense absorption bands at 1435 and 1574 cm^{-1} were assigned to the symmetric and asymmetric stretching modes of bidentate carboxylate groups, characteristic of aluminum stearate moieties (Egerton et al., 2005). Furthermore, the two intense peaks centered at 1535 and 1380 cm^{-1} could be interpreted in two ways: they might correspond to the bending of hydroxyl residues caused by moisture and the hygroscopic nature of ZnO, or alternatively to the stretching vibrations of surface-bound carboxylate groups (COO^-). The presence of carboxylate peaks on uncoated ZnO has been reported in the literature and is often attributed to residual carbon-containing species from the synthesis process, as shown by Xiong et al. (2006), who observed similar FTIR features on plasma-synthesized ZnO nanoparticles. In our case, both Zano®10 and Zano®M are uncoated according to the manufacturer, and such surface-bound carboxylates likely arise from synthesis residues or adsorption from ambient air. Additionally, bands in the 400-700 cm^{-1} region were attributed to Ti–O stretching and Ti–O–Ti bridging stretching modes (Praveen et al., 2014). FTIR spectra of Zano®M and Zano®10 also exhibited a broad absorption band around 3400 cm^{-1} associated with the stretching vibrations of hydroxyl groups. The bands within the 400-600 cm^{-1} region were assigned to the Zn–O stretching vibrations (Mahalakshmi et al., 2020). Furthermore, two intense peaks centered at 1535 and 1380 cm^{-1} could be interpreted in two ways: they may corresponded to the bending vibration of hydroxyl groups due to moisture absorption-reflecting the hygroscopic nature of ZnO-or, alternatively, to the stretching vibrations of carboxylate (COO^-) groups, depending on the particle synthesis method (Xiong et al., 2006).

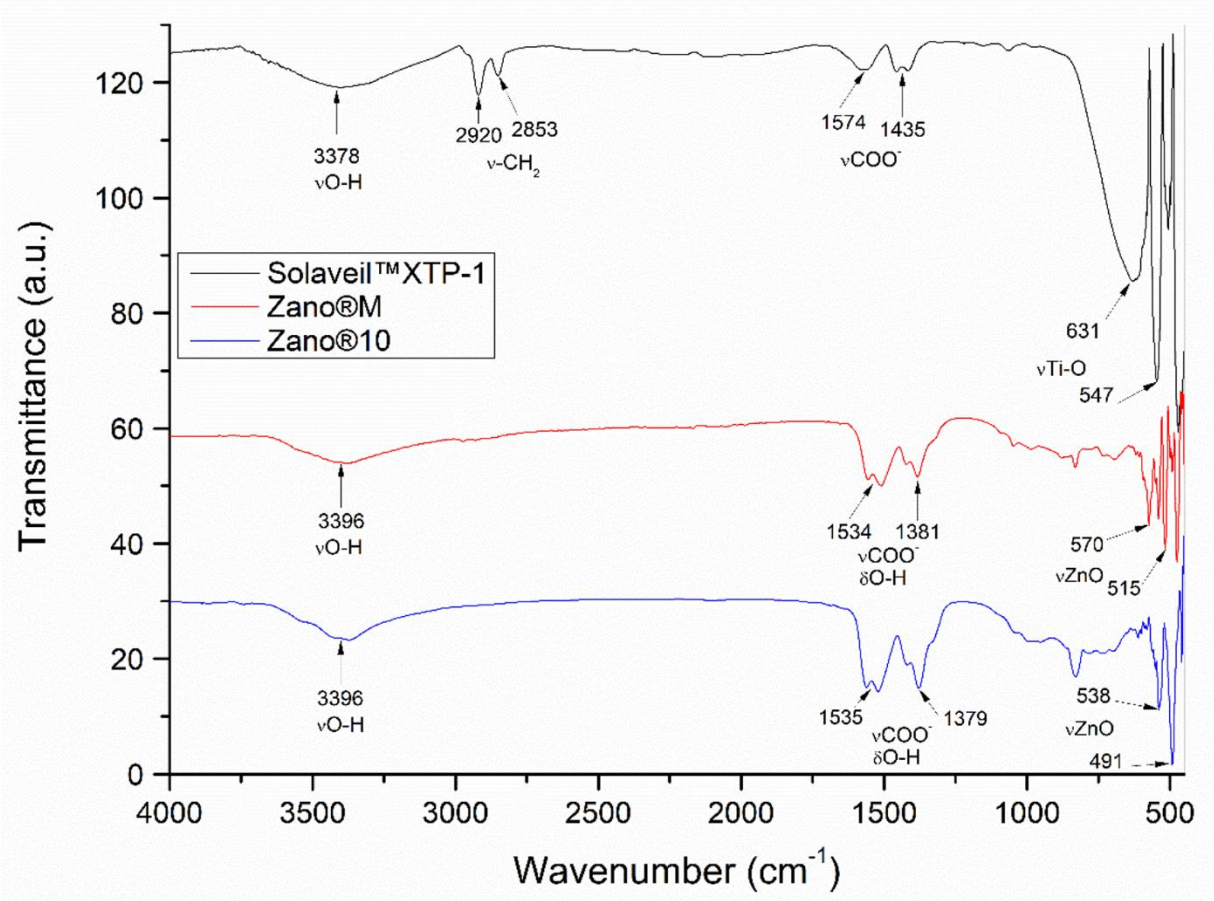

Figure 1. Normalized FTIR spectra of Solaveil™ XTP1 (black), Zano®M (red), and Zano®10 (blue) recorded in powder form. For Solaveil™ XTP1, characteristic peaks at 2853 and 2920 cm⁻¹ indicate CH_2 stretches of stearate groups, while bands at 1435 and 1574 cm⁻¹ correspond to bidentate carboxylates from aluminum stearate coating. Peaks between 400–700 cm⁻¹ reflect Ti–O and Ti–O–Ti vibrations. Zano®10 and Zano®M show broad OH stretching bands (~3400 cm⁻¹) and Zn–O stretching bands in the 400–600 cm⁻¹ range.

The morphology and size range of primary particles were determined using SEM/TEM imaging (Figure 2); results are synthetized in Table 1. Solaveil™ XTP_1 NPs has a cylindrical rounded shape, with a measured mean size of 64 ± 22 nm. Zano®M can be classified as a micromaterial with measured mean size around 244 ± 100 nm. Its exhibits various morphologies, including cylindric, hexagonal and cubic shapes. Zano®10 particles were more heterogenous, consisting of two populations as a mix of cylindrical-shaped NPs and much larger spikes-shaped particles clearly visible on TEM and SEM images. The measured mean size around 62 ± 24 nm. DLS analysis provided hydrodynamic diameter and ZP values of suspended particle agglomerates in FASW at the highest concentration. The suspended particles of Zano®10 and Solaveil™ XTP1 exhibited similar volume-weighted hydrodynamic sizes, with mean diameters of 238 ± 19 nm and 250 ± 16 nm, respectively, while

Zano®M particles formed larger agglomerates of 411 ± 52 nm. The corresponding polydispersity indices (PDI) were 1 for Zano®10, 0.86 for Zano®M, and 0.33 for Solaveil™ XTP1, reflecting the highly polydisperse nature of the ZnO suspensions and the more moderate heterogeneity of the TiO_2 suspension. These values are consistent with the known aggregation behaviour of uncoated ZnO particles in seawater and support the interpretation of the DLS size data in the context of strongly polydisperse systems.

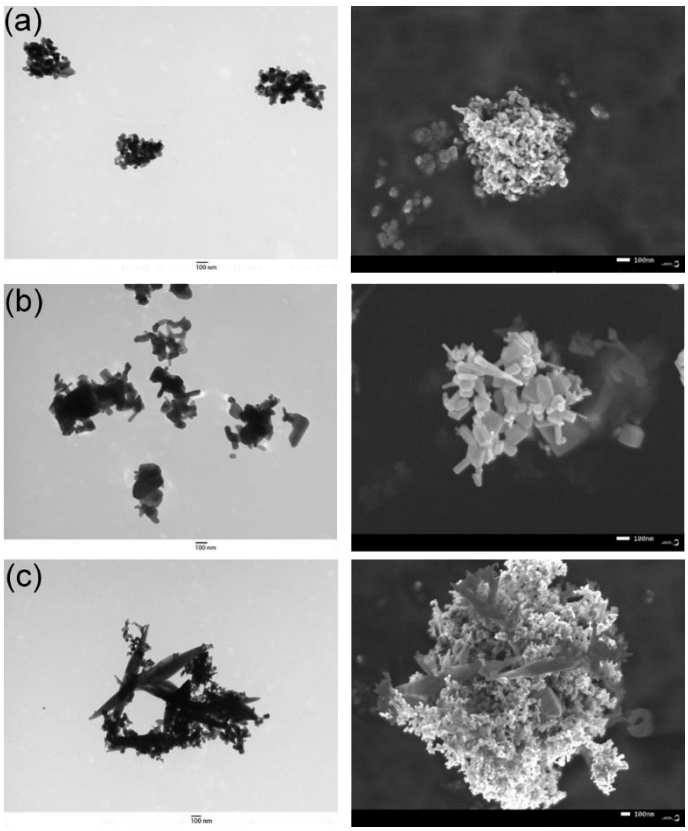

Figure 2. Transmission electron microscopy (TEM, left) and scanning electron microscopy (SEM, right) images of Solaveil™ XTP1 (a), Zano®M (b), and Zano®10 (c) primary particles. Solaveil™ XTP1 appears as homogeneous cylindrical-rounded nanoparticles with a mean diameter of ~64 nm. Zano®M exhibits a heterogeneous morphology, including cylindrical, hexagonal, and cubic micrometric particles (~245 nm average). Zano®10 presents a bimodal distribution: small cylindrical nanoparticles (~60 nm) and larger spiky-shaped particles are clearly distinguishable. All samples show evidence of agglomeration, particularly for Zano®M and Zano®10. Scale bars represent 100 nm; magnifications: TEM ×50,000 (a,b) and ×40,000 (c); SEM ×50,000 (a,b) and ×35,000 (c).

Table 1. Mineral filters characteristics

Mineral filter	Primary size (nm)	Hydrodynamic size (nm)	ZP (mV)	Morphology
Solaveil™ XTP_1	64 ± 22	250 ± 16	- 6.3	Cylindrical rounded
Zano®10	62 ± 24	238 ± 19	- 9,6	Mix of cylindric and spike

Zano®M	245 ± 100	411 ± 52	- 8,5	Mix of cylindric, hexagonal and cubic

3.2 Compared effect of mineral filters on coral metabolomes

Differential metabolomic analysis comparing exposed and control *P. damicornis* extracts revealed 44 ions with significantly altered relative concentrations ($p < 0.05$, $Log_2(FC) > 1$ or < -1) after seven days of exposure to TiO_2 and ZnO. These included 2 ions for Solaveil™ XTP_1, 18 ions for Zano®M, and 24 ions for Zano®10 exposure. All MS and MS/MS data used for metabolite annotations are provided as Supplementary Data (SI, figures S6-S69). Exposure to TiO_2-based product Solaveil™ XTP_1 induced only minimal changes in the coral metabolome, with the relative concentration of a single compound, namely monogalactosyldiacylglycerol (MGDG) $C_{18:1}/C_{16:0}$, showing a modest increase ($p = 2.6 \times 10^{-2}$, $Log_2(FC) = 1.82$) (SI, Figures S6–S8). In contrast, Zano®10 exposure led to more pronounced effects: 24 altered ions were manually annotated as 15 distinct metabolites, detailed in Table 2.

Compounds **1**-**9** were annotated as pigments. The fragmentation patterns of compounds **1** and **2** were characteristic of carotenoids and matched the MS/MS fragmentation of a β-carotene standard (SI, figure S69). These compounds were annotated as two isomers of pyrrhoxanthin, with the molecular formula $C_{39}H_{48}O_6$ (calculated *m/z* for $C_{39}H_{49}O_6^+$ 613.3524, 16 double-bond equivalents), as previously described by Clergeaud et al. (2023). The structural similarity of pyrrhoxanthin to peridinin, along with comparable fragmentation profiles (Venn et al., 2006), suggests these compounds may be structurally related to peridinin.

Compounds **3**-**5** ionized as radical cations with a molecular formula of $C_{40}H_{54}O_2$ (calculated *m/z* for $C_{40}H_{54}O_2^{+\bullet}$ 566.4118, 14 double-bond equivalents). According to the DNP database, this formula corresponds to several natural compounds, including β-carotene derivatives, diatoxanthin, and eschscholtzxanthin. Based on compound class proposals from SIRIUS and CANOPUS (classification scores of **77**%, 54% and 66%), these ions were annotated as three isomeric xanthophylls. Their ionization as cation radicals in ESI^+ mode and the successive loss of methyl radicals in the MS/MS spectra (*e.g.*, *m/z* 566.411 to 551.388, and *m/z* 474.347 to 459.324) indicate the presence of methyl substituents near a conjugated π system, consistent with observation by Crupi et al. (2010). Compounds **6**-**9** exhibited MS/MS patterns indicative of chlorophyll-derives. Each showed a phorbine

core (with four nitrogen atoms) and prominent losses of methyl and carbonyl groups. These patterns suggested a dephytylated chlorophyl structure, further supported by matches to molecular formulas in the DNP database. The only known natural compound matching the molecular formula of compound **6** is pyrophaeoporphyrin c^1, a derivative of chlorophyll c^1 described by Harradine and Maxwell (1998). Compound **7** shared its formula with 13^2,17^3-cyclopheophorbide *a* enol, previously isolated from the zooxanthellae of *Montipora digitata* (Suzuki et al., 2015). Isomeric compounds **8** and **9** had the same molecular formula as chlorophyllone *a*, a recognized chlorophyll *a* degradation product (Porphyrin 91% CANOPUS classification score) (Sakata et al., 1990). Based on their fragmentation patterns and structural predictions by SIRIUS, compounds **6**-**9** were annotated as chlorophyll degradation products.

The second group of annotated compounds (**10**-**12**) was identified as membrane lipid metabolites based on their molecular formulas and manual interpretation of their MS/MS fragmentation patterns. Compounds **10** and **11** were manually annotated as a ceramide and a glycosphingolipid (GSL) respectively, based on characteristic fragmentations of their fatty acid chains and dehydration events. Compound **10** ($C_{38}H_{71}NO_3$, calculated *m/z* for $C_{38}H_{71}NO_3Na^+$ 612.5326, 4 degrees of unsaturation) was annotated as follows: the collision-induced dissociation (CID) spectrum of [**10**+H–H_2O]$^+$ at *m/z* 572.5403 revealed a second water loss yielding a product at *m/z* 554.5308 (Figure S25). The same precursor ion also generated a fragment at *m/z* 312.3265, corresponding to a protonated $C_{20:0}$ amide, and another at *m/z* 278.2482 ($C_{18}H_{32}NO^+$), indicative of the loss of the C20:0 chain. This ion subsequently lost water (*m/z* 260.2371, $C_{18}H_{30}N^+$) and ammonia (*m/z* 260.2371, $C_{18}H_{27}^+$) confirming the annotation of compound **10** as a ceramide featuring a $C_{18:3}$;O_2 sphingoid base and a $C_{20:0;}$O fatty acid. Similarly, compound **11** was identified as a GSL based on a visible hexose loss in its MS/MS spectrum (*m/z* 770.6182 to 590.5520, – $C_6H_{12}O_6$), along with two specific products at *m/z* 328.3219 ($C_{20}H_{42}NO_2^+$) and 280.2635 ($C_{18}H_{34}NO^+$) attributed to an *N*-linked hydroxylated $C_{20:0}$;O_2 moiety and a dehydrated $C_{18:2}$ sphingoid base, respectively. It was therefore annotated as HexCer $C_{18:2}$;O/$C_{20:0}$;O_2.

An ion at *m/z* 397.3828 (calculated. for $C_{29}H_{47}^+$, 397.3829) was found at higher relative concentration in exposed coral. The MS/MS spectrum matched that of β-sitosterol in the GNPS database. To investigate further, the MS/MS spectrum of compound **12** was compared with that of a protonated dehydrated β-sitosterol standard (SI, Figure S30). Despite a strong spectral similarity, the shorter

retention time of compound **12** suggested it it be a more polar β-sitosterol derivative. Additionally, no adduct of the molecular ion was observed in the mass spectrum, limiting the accuracy of its structural annotation. Compounds **13-15** exhibited fragmentation patterns similar to those of compound **12** and the β-sitosterol standard, suggesting they were also steroids. Their molecular formulas matched several known sterol derivatives. This hypothesis is supported by previous reports on ergosterol derivatives in *Pocillopora damicornis* with comparable MS/MS spectra (Stien et al., 2020).

The fragmentation of these compounds was dominated by successive losses of water molecules. Compound **13**, with a molecular formula of $C_{29}H_{50}O_4$ (calcd. for $C_{29}H_{50}O_4Na^+$, 485.3601, 5 degrees of unsaturation), exhibited three dehydration steps, as evidenced by fragments at *m/z* 445.3678 $[M+H–H_2O]^+$, *m/z* 427.3572 $[M+H–2H_2O]^+$, and *m/z* 409.3457 $[M+H–3H_2O]^+$. Interestingly, a polyhydroxylated steroid with the same formula was previously isolated from the soft coral *Litophyton mollis* (Zovko Končić et al., 2016).

Compound **14** ($C_{35}H_{60}O_9$, calcd. *m/z* for $C_{35}H_{60}O_9Na^+$ 647.4130, 6 degrees of unsaturation) is likely a heterosidic derivative of compound **13**. Its protonated molecular ion fragmented in the source to yield a product ion at *m/z* 445.3677, corresponding to the $[M–C_6H_{12}O_6+H]^+$ ion. This ion exhibited the same collision-induced fragmentation spectrum as $[\mathbf{13}–H_2O+H]^+$. Compound **15** ($C_{29}H_{50}O_5$, calcd. *m/z* for $C_{29}H_{49}O_4^+$ 461.3626, 5 degrees of unsaturation) displayed two dehydration sites, as indicated by the ions at *m/z* 461.3626 $[M+H–H_2O]^+$ and *m/z* 443.3520 $[M+H–2H_2O]^+$. Given its formula and dehydration pattern, compound **15** was also considered as a steroid, consistent with known natural products.

The relative concentration of all annotated pigments (**1-9**) significantly decreased following exposure to Zano®10 exposure at 300 µg.L^{-1} and above, with Log_2(FC) values ranging from - 1.6 to - 4.5. Membrane lipids metabolites (**10-12**) also showed moderate decreases starting at 1000 µg.L^{-1}, with Log_2(FC) values ranging from -1.1 to -2.1. In contrast, steroids **13-15** showed significantly increased relative concentrations at the highest Zano®10 concentrations tested, with Log_2(FC) values ranging from 4.50 to 5.36.

Table 1. List of P. damicornis *metabolites with significantly altered relative concentrations after 7 days of exposure to 5, 50, 300, 1000 µg.L^{-1} of Zano®10, compared to control conditions (Log$_2$(FC) > 1 or < –1, p < 0.05).*

Cmpd. No.	Log$_2$(FC) (µg.L^{-1})[a]				RT (min)	Adduct	Exp. *m/z*	Th. *m/z*	Molecular formula	Compound class	Annotation[b]
	5	50	300	1000							
Pigments											
1	-0.72	-1.13	-4.23	-4.2	11.06	$[M+Na]^+$	635.335	635.3343	$C_{39}H_{48}O_6$	Carotenoid	Pyrrhoxanthin or isomer
2	-0.91	-0.75	-3.69	-3.64	10.93	$[M+H]^+$	613.352	613.3524	$C_{39}H_{48}O_6$	Carotenoid	Pyrrhoxanthin or isomer
3	-0.57	-0.62	-1.81	-1.65	12.07	$[M]^+$	566.4113	566.4118	$C_{40}H_{54}O_2$	Carotenoid	Xanthophyll
4	-0.62	-0.54	-1.95	-1.71	12.46	$[M]^+$	566.412	566.4118	$C_{40}H_{54}O_2$	Carotenoid	Xanthophyll
5	-0.75	-0.72	-1.64	-1.77	12.65	$[M]^+$	566.4119	566.4118	$C_{40}H_{54}O_2$	Carotenoid	Xanthophyll
6	-0.55	-1.6	-4.49	-3.95	11.32	$[M+H]^+$	529.2235	529.2234	$C_{33}H_{28}N_4O_3$	Chlorophyll derivative	n.d.
7	-0.74	-1	-2.55	-2.87	15.28	$[M+H]^+$	561.2494	561.2496	$C_{34}H_{32}N_4O_2$	Chlorophyll derivative	n.d.
8	-1.09	-1.3	-3.34	-3.36	10.45	$[M+H]^+$	533.2547	533.2547	$C_{33}H_{32}N_4O_3$	Chlorophyll derivative	n.d.
9	-1.08	-1.24	-3.19	-3.44	10.61	$[M+H]^+$	533.2548	533.2547	$C_{33}H_{32}N_4O_3$	Chlorophyll derivative	n..d.
Membrane lipids											
10	-0.58	-0.48	-0.35	-1.05	16.22	$[M+Na]^+$	612.5324	612.5326	$C_{38}H_{71}NO_3$	Ceramide	Cer $C_{18:3}$;O_2/$C_{20:0}$;O
11	-1.34	-0.56	-0.73	-2.08	14.12	$[M+Na]^+$	792.5955	792.596	$C_{44}H_{83}NO_9$	GSL	HexCer $C_{18:2}$;O/$C_{20:0}$;O_2
12	-0.15	0.32	0.03	-1.81	11.43	Frag. ($C_{29}H_{47}^+$)	397.3828	397.3829	n.d.	Steroid	β-sitosterol derivative
Steroids (putative ergosterol analogs)											
13	-0.96	2.67	1.75	4.49	10.67	$[M+Na]^+$	485.3603	485.3601	$C_{29}H_{50}O_4$	Steroid	n.d.
14	-0.53	2.25	1.2	4.5	8.56	$[M+Na]^+$	647.4131	647.4130	$C_{35}H_{60}O_9$	Steroid	n.d.
15	0.2	2.27	1.04	5.36	9.62	$[M+H–H_2O]^+$	461.3625	461.3626	$C_{29}H_{50}O_5$	Steroid	n.d.

[a]*A color gradient is applied to the Log$_2$(FC) values, ranging from dark green to yellow for metabolites whose relative concentration decreased (Log$_2$(FC) < –1), and from light orange to dark red for those whose relative concentration increased (Log$_2$(FC) > +1) after exposure to Zano®10. The color is only applied at exposure concentrations that have induced significant variation (p < 0.05).* [b]*For the ceramide and the glycosphingolipid (GSL), chain lengths were visible in the MS/MS spectra but the position of double bonds in the sphingoid base remained speculative and is therefore deliberately omitted in the annotations. n.d.: not determined.*

A total of 12 metabolites with altered relative concentration after exposure to Zano®M were annotated and are listed in Table 3. These include pyrrhoxanthins **1-2** and GSL **11** already annotated above. Compound **16** MS/MS spectrum was similar to that of compound **11**, allowing for the annotation of **16** as the GSL HexCer $C_{19:2}$;O/$C_{16:0}$;O_2. Compound **17** was annotated as the DGDG $C_{18:2}$/$C_{16:0}$ as in previous work (Marcellin-Gros et al., 2020). Compounds **18-20** were manually annotated based on their characteristic fragments at *m/z* 104.1070 and 132.1021 visible in the $[M+H]^+$ MS/MS spectrum

as well as the visible loss of C_3H_9N in the $[M+Na]^+$ MS/MS spectrum (Marcellin-Gros et al., 2020). Eventually, compound **18** was annotated as the lyso-DGCC $C_{22:6}$, **19** as the DGCC $C_{22:6}/C_{22:6}$, and **20** as the DGCC $C_{16:0}/C_{18:4}$. Compound **21** matched to LPC $C_{22:6}$ in the GNPS database. This assertion is corroborated by the observation of a phosphocholine ion at *m/z* 184.0736 in the MS/MS fragmentation spectrum of its protonated molecular ion (Stien et al., 2020). Compound **22** was annotated as L-tryptophan. The annotation was confirmed by comparison with an analytical standard (SI, Figures S59-60). Compounds **23** and **24** remained unidentified but appeared to be analogs of each other. Overall, the coral metabolome was significantly affected by exposure to Zano®M only at the highest tested concentration of 1000 µg.L^{-1}.

Lastly, the only compound whose relative concentration was affected following exposure to Solaveil™ XTP_1 was annotated as MGDG $C_{18:1}/C_{16:0}$, already observed in a previous publication (Marcellin-Gros et al., 2020). As the alteration of a single metabolite does not constitute a significant response signal, it can be concluded that Solaveil™ XTP_1 had no measurable effect on the metabolome of adult corals at 1000 µg.L^{-1} exposure.

Table 2. List of P. damicornis *metabolites with significantly altered relative concentrations after 7 days of exposure to 5, 50, 300, 1000 µg.L^{-1} of Zano®M, ($Log_2(FC) > 1$ or < -1, $p < 0.05$).*

Cmpd. No.	$Log_2(FC)$ (µg.L^{-1})[a] 5	50	300	1000	RT (min)	Adduct	Exp. *m/z*	Th. *m/z*	Molecular formula	Compound class[b]	Annotation[c]
Pigments											
1	0.87	0.03	-1.61	-1.55	10.66	$[M+H]^+$	613.3523	613.3524	$C_{39}H_{48}O_6$	Carotenoid	Pyrrhoxanthin or isomer
2	0.66	0.09	-1.08	-2.58	10.48	$[M+H]^+$	613.3523	613.3524	$C_{39}H_{48}O_6$	Carotenoid	Pyrrhoxanthin or isomer
Membrane lipids											
11	-0.27	-0.21	-0.24	-1.25	15.04	$[M+Na]^+$	792.5963	792.596	$C_{44}H_{83}NO_9$	GSL	HexCer $C_{18:2}$;O/$C_{20:0}$;O_2
16	-1.24	-0.21	-0.4	-1.02	12.14	$[M+Na]^+$	750.5475	750.549	$C_{41}H_{77}NO_9$	GSL	HexCer $C_{19:2}$;O/$C_{16:0}$;O_2
17	2.98	2.93	1.08	3.66	13.28	$[M+Na]^+$	939.6013	939.602	$C_{49}H_{88}O_{15}$	DGDG	DGDG $C_{18:2}/C_{16:0}$
18	-1.18	-0.79	-0.53	-1.17	7.06	$[M+H]^+$	562.3738	562.374	$C_{32}H_{51}NO_7$	LDGCC	LDGCC $C_{22:6}$
19	-0.61	-0.6	-0.18	-1.03	11.99	$[M+H]^+$	872.6042	872.604	$C_{54}H_{82}NO_8$	DGCC	DGCC $C_{22:6}/C_{22:6}$
20	-0.07	0.1	0.3	1.38	12.73	$[M+H]^+$	748.5729	748.572	$C_{44}H_{77}NO_8$	DGCC	DGCC $C_{16:0}/C_{18:4}$
21	-0.81	-0.49	-0.83	-1.05	7.45	$[M+H]^+$	568.3398	568.340	$C_{30}H_{50}PNO_7$	LPC	LPC $C_{22:6}$
Amino acid											
22	-0.72	-0.45	-0.42	-1.03	4.22	$[M+H]^+$	205.0971	205.097	$C_{11}H_{12}N_2O_2$	Amino acid	L-Tryptophane
Unidentified											
23	-0.63	-0.39	0.02	-1.5	14.52	$[M+Na]^+$	571.4331	571.433	$C_{34}H_{60}O_5$	n.d	n.d

24	-0.55	-0.57	-0.05	-1.48	15.57	$[M+Na]^+$	573.4489	573.449	$C_{34}H_{62}O_5$	n.d	n.d

[a]A color gradient is applied to the $Log_2(FC)$ values, ranging from dark green to yellow for metabolites whose relative concentration decreased ($Log_2(FC) < -1$), and from light orange to dark red for those whose relative concentration increased ($Log_2(FC) > +1$) after exposure to Zano®M. The color is only applied at exposure concentrations that have induced significant variation ($p < 0.05$). [b]DGDG: digalactosyldiacylglycerol, LDGCC: lysodiacylglyceryl carboxyhydroxymethylcholine, DGCC: diacylglyceryl carboxyhydroxymethylcholine, LPC: lysophosphatidylcholine, GSL: glycosphingolipid, nd: non determined. [c]For DGDG, LDGCC, DGCC, GSL and LPC, chain lengths were visible in the MS/MS spectra but the position of double bonds remained speculative and is, therefore, deliberately omitted in the annotations.

4. Discussion

The present study investigated the effects of three mineral UV filters using an untargeted metabolomic approach, complemented by detailed particle characterization, to provide a more comprehensive understanding of their potential mechanisms of toxicity. Each mineral filter showed a tendency to form agglomerates with low negative zeta potential (ZP) values, approximating those of the FASW medium, indicating weak electrostatic repulsion and a high likelihood of aggregation. The formation of agglomerates in FASW was further confirmed by hydrodynamic size measurements, with agglomerate diameters exceeding 200 nm for Solaveil™ XTP_1 and Zano®10 NPs, and 400 nm for Zano®M. The fate of these agglomerates may vary depending on their intrinsic physical and chemical properties.

For Solaveil™ XTP_1 NPs, it is likely that the agglomerates did not interact substantially with the exposed corals, as no polyp retraction was observed after seven days of exposure (SI, figure S1). Polyp retraction is a morphological colony-scale response observed in corals under stress, acting as a protective mechanism to limit contact with adverse environmental conditions (Bejarano et al., 2022). This behavior has also been reported in previous studies involving exposure to UV filters (Miller et al., 2022; Stien et al., 2019). This limited interaction is further corroborated by the negligible impact of Solaveil™ XTP_1 on the coral metabolome. The minimal effect may be attributed to the buoyant properties of the particles in FASW. Slomberg et al. (2021) reported that TiO_2 particles coated with aluminum and stearic acid remain at the water surface due to their hydrophobic coating. Consistently,

TiO_2 quantification in marine ecosystems has shown peak concentrations near the surface (Labille et al., 2020; Thallinger et al., 2023; Tovar-Sánchez et al., 2013). These findings suggest that Solaveil™ XTP_1 may not reach coral nubbins for seven days exposure, explaining the limited metabolic and behavioral responses observed. In contrast, Zano®10 and Zano®M exposure resulted in marked coral responses with full polyp retraction observed within 24 hours at 1000 µg.L^{-1} (SI, Figures S2-S3). Once dispersed in FASW, these agglomerates likely sediment through the water column, possibly causing mechanical stress via direct physical contact with the coral surface or through ingestion, ultimately reaching the gastrodermal tissues (Tang et al., 2017; Yuan et al., 2023). In addition, these particles may release Zn^{2+} ions into the water, contributing to chemical toxicity (Freitas Neto and Espósito, 2023).

Untargeted metabolomics analysis allowed the annotation of various metabolites affected by the two ZnO particles, revealing distinct trends. Significant metabolome shifts were mainly observed for Zano®10 which led to a decrease in the relative abundance of several pigments including carotenoids, xanthophylls and chlorophylls metabolites at 300 and 1000 µg.L^{-1}. Most of these pigments originate from Symbiodiniaceae and are essential for photosynthetic energy production (Kopp et al., 2015). Variations in photosynthetic pigment levels are commonly used as reliable indicators of environmentally induced stress in corals (McDougall et al., 2006; Scheufen et al., 2017). The major light-harvesting pigments in Symbiodiniaceae include peridinin and chlorophylls, which bind to antennae proteins to form Peridinin–Chlorophyll Proteins (PCPs) (Jiang et al., 2012). Chlorophyll in particular was widely used as a bioindicator to assess the density of unicellular photosynthetic organisms such as *Symbiodinium spp.* (Ramsby et al., 2014; Zhou et al., 2022). Furthermore, decreased levels of pyrrhoxanthin, a structural analog of peridinin, were previously reported in *P. damicornis* exposed to 300 and 1000 µg/L of avobenzone (butyl methoxydibenzoylmethane), indicating potential disruption of symbiont integrity (Clergeaud et al., 2023). In the present work, the marked loss of photosynthetic pigments following Zano®10 exposure suggested a direct damage to the PCP complex or a reduction in Symbiodiniaceae density, suggesting impairment of the photosynthetic machinery. In contrast, Solaveil™ XTP_1 had no detectable impact on the pigmental composition. A decrease in pyroxanthin derivatives was also observed in corals exposed to 1000 µg.L^{-1} Zano®M.

These results are consistent with literature reporting stronger impacts of ZnO particles compared to coated TiO_2. Corinaldesi et al. (2018) showed that exposure to 6.3 $mg.L^{-1}$ of uncoated ZnO NPs (20 to 200 nm) induced massive expulsion of damaged zooxanthellae in *Acropora* spp. within 24 hours. Conversely, lesser effects were reported with coated TiO_2 NPs (Eusolex® T2000 and Optisol™), where only minor zooxanthellae release and no visible bleaching were observed after 48 hours.

Fel et al. (2019) also observed reduced photosynthetic efficiency in *Stylophora pistillata* exposed to 100 $\mu g.L^{-1}$ ZnO for 35 days, suggesting damage to photosystem II (PSII), although the particle characteristics were not fully defined. Similar observations were made by Chen et al. (2025), who investigated the acute toxicity of ZnO (800 $\mu g.L^{-1}$, 20–40 nm) and TiO_2 (30 $mg.L^{-1}$, 40–60 nm) NPs on *Galaxea fascicularis* coral for 48 hours, revealing a significant impairment of Symbiodiniaceae functions, characterized by a decrease in chlorophyll content and a reduction in photosynthetic capacity for both NPs. These effects were associated with oxidative stress-induced damage, with ZnO NPs exhibiting a more pronounced deleterious impact despite their lower concentration. In this study, the metabolomic profile of corals exposed to Zano®10 indicate early signs of bleaching, reinforcing the idea that nanoparticle size plays a critical role in toxicity. Zano®M, being larger particles, was comparatively less toxic. The relationship between size and toxicity has been well-documented in photosynthetic organisms such as algae: smaller particles have a larger surface area, which may facilitate interaction with or uptake into cell membranes, leading to cellular deformation and increased permeability (Chen et al., 2012; Djearamane et al., 2019), reduced pigment contents (Djearamane et al., 2018), and metabolic deficiency (Elrefaey et al., 2021), all of which can precede potential damage to the photosynthetic apparatus. Moreover, the dissolution rate of uncoated metal oxide NPs like ZnO is size-dependent, with smaller particles dissolving faster and releasing more bioavailable Zn^{2+} ions (Wu et al., 2019). Smaller NPs dissolve more quickly, release bioavailable Zn^{2+} ions into the medium, and affect the photosynthetic homeostasis of exposed organisms. Trace concentrations of Zn^{2+} ions are essential enzyme cofactors and play a key role in photosynthetic efficiency of corals symbionts (Ferrier-Pagès et al., 2005), while excessive concentrations can adversely affect this biological function and enhance bleaching process. Kuzminov et al. (2013) demonstrated that Zn accumulation can lead to electron transport and growth inhibition in *Symbiodinium* spp. after two days of exposure to 100 µM of Zn. Zn^{2+} poisoning has also had a detrimental effect on the pigment composition of

marine microalgae, as evidenced by a decrease in chlorophyll *a* content in *Chlorella marina*, *Isochrysis galbana*, *Tetraselmis* sp., *Nannochloropsis* sp. and *Dunaliella salina* following 15 days exposure to 500 ppm of dissolved Zn (Dinesh et al., 2014). In symbiotic cnidarians, zinc is primarily absorbed by the zooxanthellae, as shown by Hardefeldt and Reichelt-Brushett (2015) in the sea anemone *Exaiptasia pallida*, and by Reichelt-Brushett and McOrist (2003) in the hermatypic coral *Acropora tenuis*. This partitioning acts as a metal regulation mechanism but may also contribute to bleaching via metabolic deterioration of cells or the enhanced expulsion of Zn^{2+} contaminated zooxanthellae. Both particulate and ionic forms of zinc can trigger the formation of reactive oxygen species (ROS) in photosynthetic organisms, leading to oxidative damage that impairs cellular components, and compromises structural integrity (Vicente et al., 2018). Chen et al. (2025) observed a significant increase in ROS activity in *Galaxea fascicularis* after 48 hours of exposure to both 800 $\mu g \cdot L^{-1}$ ZnO nanoparticles and 30 $mg \cdot L^{-1}$ TiO_2 in coral tissues, suggesting a potential contribution of ROS to the bleaching effects observed for both tested NPs. ROS production is a well-documented factor in coral bleaching, particularly in response to thermal stress (Lesser, 2019; Strohecker et al., 2021), may contribute to the observed changes in pigment or lipid profiles.

Zano®M exhibited a weaker effect on coral metabolome, with only moderate variations observed at the highest concentration tested (1000 $\mu g.L^{-1}$). The metabolomic analysis showed that exposure primarily affected the relative concentrations of membrane lipids in Symbiodiniaceae. In addition to pigments, corals possess a diverse and complex lipid profile, with varying structures and ratios depending on the taxa of both symbiotic zooxanthellae and coral host (Reddy et al., 2023). For Zano®10 exposure, the few membrane lipids annotated as symptomatic of exposure were one ceramide, one GSL, and four phytosteroids. In contrast, Zano®M exposure induced a broader variation in lipid metabolites (**11**-**21**), involving metabolites specifically associated with the *Symbiodinium* spp. membrane lipidome. Symbiont membrane properties and integrity are strongly influenced by lipid composition, which can be modulated in response to environmental pressures, especially during coral bleaching events (Ermolenko and Sikorskaya, 2021; Sikorskaya et al., 2020; T. Botana et al., 2022; Tang et al. 2014a), but this phenomenon has also been observed as an acclimatization response in scleractinian corals under chemical stress (Tang et al. 2014b). Variation in betaine lipids, such as DGCCs, may indicate a

reorganization of the symbiont's membrane lipids. These metabolites are often associated with the thermotolerance capacity of different zooxanthellae clades (Rosset et al. 2019; Roach et al. 2021), particularly by modulating the structure of the cellular membrane (Pei et al., 2022). In a context of particles exposure, Tang et al (2017) highlighted cellular adaptation to mechanical disturbances in the coral *Seriatopora caliendrum* exposed to uncoated ZnO NPs (50–70 nm). They observed changes in phosphatidylcholine content at 50 $\mu g.L^{-1}$, but only in response to particles exposure and not to dissolved Zn^{2+} ions. Additionally, they identified a variation in LPC 22:6 (compound **21**) relative concentration, a metabolite found in tissues of various species, including corals (Tang et al., 2014b; Williams et al., 2024), where it may influence membrane fluidity and permeability, particularly in response to NP-induced physical damages. Unlike Zano®10 NPs, which significantly affected pigment content, Zano®M particles seem to primarily interacted mechanically with the coral surface, accounting for the observed variation in lipid relative concentrations. The larger agglomerates formed by Zano®M may have reduced the contact area between the particles and the coral while also promoting sedimentation, thereby decreasing their bioavailability.

Other metabolites were annotated in this study, including three polar ergosterol derivatives, whose relative concentration increased following Zano®10 exposure. Symbiotic cnidarians acquire sterols from their symbionts and/or diet, which are essential for cell maintenance and immune signaling (Hambleton et al., 2019; Lu et al., 2020). Ergosterol derivatives are widespread across the animal kingdom, including in soft corals (Savić et al., 2022), and play diverse roles due to their highly variable structures and involvement in multiple metabolic pathways. However, interpreting their biological significance remains challenging, as sterol functions in corals are not yet well understood, and their precise structures have not been identified. Increased steroids relative concentration was previously associated to an inflammatory stress response of *P. damicornis* exposed to the UV filter ethylhexyl salicylate (Stien et al., 2020). Notably, this study did not identify the same steroids or other metabolites previously associated with an inflammatory response in corals. This suggests that Zano®10 toxicity does not affect the same partner within the coral symbiosis. Based on the variations in the relative concentrations of pigments, it appears that Zano®10 toxicity primarily targets Symbiodiniaceae.

Finally, a slight decline in the relative concentration of the amino acid L-tryptophan was observed following Zano®M exposure. Tryptophan biosynthesis is primarily associated with the Symbiodiniaceae (Liu et al., 2018). In photosynthetic organisms, tryptophan is commonly described as a precursor to the phytohormone indole-3-acetic acid, which plays a key role in growth and development (Palacios et al., 2016). While a single metabolite within a class provides only a weak signal, this observation suggests potential disruptions in Symbiodiniaceae metabolism.

Conclusion

The bleaching potential of mineral filters such as ZnO and TiO_2 particles has been well-documented in several studies. The present findings provide new insights into the potential toxicity mechanisms of these filters in relation to their physicochemical properties. This study revealed distinct effects of the mineral filters Solaveil™ XTP_1 (TiO_2 NPs), Zano®10 (ZnO NPs) and Zano®M (ZnO particles) on *P. damicornis* after seven days of exposure, as evidenced by alterations in the metabolite profile of the symbiotic zooxanthellae. Solaveil™ XTP_1 induced minimal changes in the coral metabolome, likely due to its hydrophobic properties that may have limited its interaction with the corals. In contrast, Zano®10 exhibited the highest toxicity, significantly reducing the relative concentration of several photosynthetic pigments at 300 and 1000 $\mu g.L^{-1}$. Zano®M, on the other hand, caused only mild effects, primarily indicative of cell membrane remodeling at 1000 $\mu g.L^{-1}$.

Further investigations into the functional biological effects of ZnO, particularly on the symbiont, could provide deeper insights into its toxicity mechanisms and contribute to assessing the safety of these compounds. While nominal concentrations were used to reflect realistic exposure scenarios, we acknowledge that quantifying the actual concentrations of dissolved Zn^{2+} or total particulate matter in the medium would have provided deeper insights into the relative contributions of ionic versus particulate toxicity. Dissolved zinc analysis typically relies on ultrafiltration followed by inductively coupled plasma mass spectrometry (ICP-MS) or atomic absorption spectroscopy (AAS), sometimes after dialysis or centrifugal separation (Li et al., 2013; Wu et al., 2019). However, the implementation of such techniques requires labor-intensive protocols and specialized equipment, especially when handling dynamic nanoparticle suspensions in complex media such as seawater. Given the already

broad scope of this study, we suggest addressing this question in future work to better distinguish the roles of ZnO particles and dissolved zinc in coral ecotoxicology. Given the anticipated rise in the use of mineral filters, continued investigations into their effects, especially considering their physicochemical characteristics, remains crucial.

Data availability

The mass spectrometry data can be accessed on the European research data repository Zenodo at https://zenodo.org/uploads/15167165, which is publicly available.

Acknowledgments.

This work was carried out with the financial support of the Agence Nationale de la Recherche, grant number ANR21-CE34-0027, SPOC project (Sunscreen Pollution on Coral). Preliminary work was financed by Pierre Fabre Dermo Cosmétique as part of their commitment to sunscreens that protect the skin and are more respectful of the oceans.

Authors thank the BIO2MAR (http://bio2mar.obs-banyuls.fr), BioPIC (https://www.embrc-france.fr) and EnRMAT (https://enrmat.univ-perp.fr) platforms for providing technical support and access to instrumentation for metabolomic profiling and particle characterization; the Softmat platform (https://softmat.fr) for DLS analysis; the European Marine Biological Resource Center (EMBRC) at the Observatoire Océanologique de Banyuls, France, for providing access to the Banyuls aquarium facilities. Finally, the authors also would like to thank Rémi Pillot and Pascal Romans (Sorbonne Université) for their help in coral rearing.

Author contributions.

CG: Investigation, Formal analysis, Writing – Original draft, Writing – Review & Editing

MG: Supervision, Validation, Writing – Original draft, Writing – Review & Editing

FC: Investigation

ET: Investigation

LC: Investigation – Review & Editing

LM: Writing – Review and Editing

PL: Conceptualization, Supervision, Project administration

EH: Supervision, Validation, Writing – Original draft, Writing – Review & Editing

DS: Conceptualization, Methodology, Validation, Supervision, Original draft, Review & Editing, Project administration

All authors contributed to and approved the final manuscript.

Competing interests

Preliminary work reported in this article was by Pierre Fabre Dermo Cosmétique as part of their commitment to sunscreens that protect the skin and are more respectful of the oceans. It was neither supervised nor audited by Pierre Fabre Laboratories. The interpretations and views expressed in this manuscript do not reflect those of the company.

References

Ahmad, M.M., Mushtaq, S., Al Qahtani, H.S., Sedky, A., Alam, M.W., 2021. Investigation of TiO2 Nanoparticles Synthesized by Sol-Gel Method for Effectual Photodegradation, Oxidation and Reduction Reaction. Crystals 11, 1456. https://doi.org/10.3390/cryst11121456

Bejarano, S., Diemel, V., Feuring, A., Ghilardi, M., Harder, T., 2022. No short-term effect of sinking microplastics on heterotrophy or sediment clearing in the tropical coral Stylophora pistillata. Sci. Rep. 12. https://doi.org/10.1038/s41598-022-05420-7

Berkelmans, R., Van Oppen, M.J.H., 2006. The role of zooxanthellae in the thermal tolerance of corals: a 'nugget of hope' for coral reefs in an era of climate change. Proc. R. Soc. B Biol. Sci. 273, 2305–2312. https://doi.org/10.1098/rspb.2006.3567

Bramanti, L., Iannelli, M., Fan, T.Y., Edmunds, P.J., 2015. Using demographic models to project the effects of climate change on scleractinian corals: Pocillopora damicornis as a case study. Coral Reefs 34, 505–515. https://doi.org/10.1007/s00338-015-1269-z

Brener-Raffalli, K., Clerissi, C., Vidal-Dupiol, J., Adjeroud, M., Bonhomme, F., Pratlong, M., Aurelle, D., Mitta, G., Toulza, E., 2018. Thermal regime and host clade, rather than geography, drive Symbiodinium and bacterial assemblages in the scleractinian coral Pocillopora damicornis sensu lato. Microbiome 6, 39. https://doi.org/10.1186/s40168-018-0423-6

Bridge, T.C.L., Hoey, A.S., Campbell, S.J., Muttaqin, E., Rudi, E., Fadli, N., Baird, A.H., 2014. Depth-dependent mortality of reef corals following a severe bleaching event: implications for thermal refuges and population recovery. F1000Research 2, 187. https://doi.org/10.12688/f1000research.2-187.v3

Cameron, L.P., Reymond, C.E., Bijma, J., Büscher, J.V., De Beer, D., Guillermic, M., Eagle, R.A., Gunnell, J., Müller-Lundin, F., Schmidt-Grieb, G.M., Westfield, I., Westphal, H., Ries,

673 J.B., 2022. Impacts of Warming and Acidification on Coral Calcification Linked to
674 Photosymbiont Loss and Deregulation of Calcifying Fluid pH. J. Mar. Sci. Eng. 10,
675 1106. https://doi.org/10.3390/jmse10081106
676 Chen, J., Yu, K., Yu, X., Zhang, R., Chen, B., 2025. Transcriptomic and physiological analyses
677 reveal the toxic effects of inorganic filters (nZnO and nTiO2) on scleractinian coral
678 *Galaxea fascicularis*. Environ. Res. 267, 120663.
679 https://doi.org/10.1016/j.envres.2024.120663
680 Chen, P., Powell, B.A., Mortimer, M., Ke, P.C., 2012. Adaptive Interactions between Zinc
681 Oxide Nanoparticles and *Chlorella* sp. Environ. Sci. Technol. 46, 12178–12185.
682 https://doi.org/10.1021/es303303g
683 Clergeaud, F., Giraudo, M., Rodrigues, A.M.S., Thorel, E., Lebaron, P., Stien, D., 2023. On the
684 Fate of Butyl Methoxydibenzoylmethane (Avobenzone) in Coral Tissue and Its Effect
685 on Coral Metabolome. Metabolites 13, 533.
686 https://doi.org/10.3390/metabo13040533
687 Connolly, M., Hernández-Moreno, D., Conde, E., Garnica, A., Navas, J.M., Torrent, F.,
688 Rucandio, I., Fernandez-Cruz, M.L., 2022. Influence of citrate and PEG coatings on the
689 bioaccumulation of TiO2 and CeO2 nanoparticles following dietary exposure in
690 rainbow trout. Environ. Sci. Eur. 34, 1. https://doi.org/10.1186/s12302-021-00581-0
691 Conway, A.J., Gonsior, M., Clark, C., Heyes, A., Mitchelmore, C.L., 2021. Acute toxicity of the
692 UV filter oxybenzone to the coral Galaxea fascicularis. Sci. Total Environ. 796, 148666.
693 https://doi.org/10.1016/j.scitotenv.2021.148666
694 Corinaldesi, C., Marcellini, F., Nepote, E., Damiani, E., Danovaro, R., 2018. Impact of inorganic
695 UV filters contained in sunscreen products on tropical stony corals (Acropora spp.).
696 Sci. Total Environ. 637–638, 1279–1285.
697 https://doi.org/10.1016/j.scitotenv.2018.05.108
698 Crupi, P., Milella, R.A., Antonacci, D., 2010. Simultaneous HPLC-DAD-MS (ESI+) determination
699 of structural and geometrical isomers of carotenoids in mature grapes. J. Mass
700 Spectrom. 45, 971–980. https://doi.org/10.1002/jms.1794
701 Danovaro, R., Bongiorni, L., Corinaldesi, C., Giovannelli, D., Damiani, E., Astolfi, P., Greci, L.,
702 Pusceddu, A., 2008. Sunscreens Cause Coral Bleaching by Promoting Viral Infections.
703 Environ. Health Perspect. 116, 441–447. https://doi.org/10.1289/ehp.10966
704 Dinesh, K., Santhanam, P., Selvaraju, A., Devi, A.S., Kumar, N., Barathan, B., Selvakumaran, J.,
705 Thillainayagam, J., Ananthi, P., 2014. Effect of different dosages of zinc on the growth
706 and biomass in five marine microalgae. Int. J. Fish. Aquac. 6, 1–8.
707 https://doi.org/10.5897/IJFA2013.0393
708 Djearamane, S., Lim, Y.M., Wong, L.S., Lee, P.F., 2019. Cellular accumulation and cytotoxic
709 effects of zinc oxide nanoparticles in microalga Haematococcus pluvialis. PeerJ 7,
710 e7582. https://doi.org/10.7717/peerj.7582
711 Djearamane, S., Lim, Y.M., Wong, L.S., Lee, P.F., 2018. Cytotoxic effects of zinc oxide
712 nanoparticles on cyanobacterium Spirulina (Arthrospira) platensis. PeerJ 6, e4682.
713 https://doi.org/10.7717/peerj.4682
714 Dührkop, K., Fleischauer, M., Ludwig, M., Aksenov, A.A., Melnik, A.V., Meusel, M.,
715 Dorrestein, P.C., Rousu, J., Böcker, S., 2019. SIRIUS 4: a rapid tool for turning tandem
716 mass spectra into metabolite structure information. Nat. Methods 16, 299–302.
717 https://doi.org/10.1038/s41592-019-0344-8.
718 Egerton, T.A., Everall, N.J., Tooley, I.R., 2005. Characterization of TiO_2 Nanoparticles Surface
719 Modified with Aluminum Stearate. Langmuir 21, 3172–3178.
720 https://doi.org/10.1021/la047390d

Elrefaey, A., El-Gamal, A., Hamed, S.M., El-Belely, E.F., 2021. Growth, primary metabolites, and cell morphogenesis of Scenedesmus opoliensis in response to zinc oxide nanoparticles stress. Egypt. J. Phycol. 22, 100–118. https://doi.org/10.21608/egyjs.2021.98243.1007

Ermolenko, E.V., Sikorskaya, T.V., 2021. Lipidome of the reef-building coral *Acropora cerealis:* Changes under thermal stress. Biochem. Syst. Ecol. 97, 104276. https://doi.org/10.1016/j.bse.2021.104276

Fel, J.-P., Lacherez, C., Bensetra, A., Mezzache, S., Béraud, E., Léonard, M., Allemand, D., Ferrier-Pagès, C., 2019. Photochemical response of the scleractinian coral *Stylophora pistillata* to some sunscreen ingredients. Coral Reefs 38, 109–122. https://doi.org/10.1007/s00338-018-01759-4.

Feng, L., Yan, Z., Shi, X., Sultonzoda, F., 2018. Anti-icing/frosting and self-cleaning performance of superhydrophobic aluminum alloys. Appl. Phys. A 124, 142. https://doi.org/10.1007/s00339-017-1509-x

Ferrier-Pagès, C., Houlbrèque, F., Wyse, E., Richard, C., Allemand, D., Boisson, F., 2005. Bioaccumulation of zinc in the scleractinian coral Stylophora pistillata. Coral Reefs 24, 636–645. https://doi.org/10.1007/s00338-005-0045-x

Freitas Neto, L., Espósito, B., 2023. TOXICITY OF ZINC OXIDE TO SCLERACTINIAN CORALS AND ZOOXANTHELLAE: A BRIEF REVIEW. Quím. Nova. https://doi.org/10.21577/0100-4042.20230003

Hambleton, E.A., Jones, V.A.S., Maegele, I., Kvaskoff, D., Sachsenheimer, T., Guse, A., 2019. Sterol transfer by atypical cholesterol-binding NPC2 proteins in coral-algal symbiosis. eLife 8, e43923. https://doi.org/10.7554/eLife.43923

Hardefeldt, J.M., Reichelt-Brushett, A.J., 2015. Unravelling the role of zooxanthellae in the uptake and depuration of an essential metal in Exaiptasia pallida; an experiment using a model cnidarian. Mar. Pollut. Bull. 96, 294–303. https://doi.org/10.1016/j.marpolbul.2015.04.055

He, T., Tsui, M.M.P., Tan, C.J., Ma, C.Y., Yiu, S.K.F., Wang, L.H., Chen, T.H., Fan, T.Y., Lam, P.K.S., Murphy, M.B., 2019. Toxicological effects of two organic ultraviolet filters and a related commercial sunscreen product in adult corals. Environ. Pollut. 245, 462–471. https://doi.org/10.1016/j.envpol.2018.11.029

J. Harradine, P., R. Maxwell, J., 1998. Pyrophaeoporphyrins c1 and c2: grazing products of chlorophyll c in aquatic environments. Org. Geochem. 28, 111–117. https://doi.org/10.1016/S0146-6380(97)00123-X

Jiang, J., Zhang, H., Kang, Y., Bina, D., Lo, C.S., Blankenship, R.E., 2012. Characterization of the peridinin–chlorophyll *a*-protein complex in the dinoflagellate *Symbiodinium*. Biochim. Biophys. Acta BBA - Bioenerg. 1817, 983–989. https://doi.org/10.1016/j.bbabio.2012.03.027

Jovanović, B., Guzmán, H.M., 2014. Effects of titanium dioxide (TiO_2) nanoparticles on caribbean reef-building coral (*Montastraea faveolata*). Environ. Toxicol. Chem. 33, 1346–1353. https://doi.org/10.1002/etc.256.

Kim, K.T., Klaine, S.J., Cho, J., Kim, S.-H., Kim, S.D., 2010. Oxidative stress responses of Daphnia magna exposed to TiO(2) nanoparticles according to size fraction. Sci. Total Environ. 408, 2268–2272. https://doi.org/10.1016/j.scitotenv.2010.01.041

Kopp, C., Domart-Coulon, I., Escrig, S., Humbel, B.M., Hignette, M., Meibom, A., 2015. Subcellular Investigation of Photosynthesis-Driven Carbon Assimilation in the Symbiotic Reef Coral *Pocillopora damicornis*. mBio 6, e02299-14. https://doi.org/10.1128/mBio.02299-14

769 Kuzminov, F.I., Brown, C.M., Fadeev, V.V., Gorbunov, M.Y., 2013. Effects of metal toxicity on
770 photosynthetic processes in coral symbionts, *Symbiodinium* spp. J. Exp. Mar. Biol.
771 Ecol. 446, 216–227. https://doi.org/10.1016/j.jembe.2013.05.017
772 Labille, J., Slomberg, D., Catalano, R., Robert, S., Apers-Tremelo, M.-L., Boudenne, J.-L.,
773 Manasfi, T., Radakovitch, O., 2020. Assessing UV filter inputs into beach waters
774 during recreational activity: A field study of three French Mediterranean beaches
775 from consumer survey to water analysis. Sci. Total Environ. 706, 136010.
776 https://doi.org/10.1016/j.scitotenv.2019.136010
777 Lai, R.W.S., Kang, H.-M., Zhou, G.-J., Yung, M.M.N., He, Y.L., Ng, A.M.C., Li, X., Djurišić, A.B.,
778 Lee, J.-S., Leung, K.M.Y., 2021. Hydrophobic Surface Coating Can Reduce Toxicity of
779 Zinc Oxide Nanoparticles to the Marine Copepod Tigriopus japonicus. Environ. Sci.
780 Technol. 55, 6917–6925. https://doi.org/10.1021/acs.est.1c01300
781 Lesser, M.P., 2019. Phylogenetic signature of light and thermal stress for the endosymbiotic
782 dinoflagellates of corals (Family Symbiodiniaceae). Limnol. Oceanogr. 64, 1852–1863.
783 https://doi.org/10.1002/lno.11155
784 Lewicka, Z., Benedetto, A., Benoit, D., Yu, W., Fortner, J., Colvin, V., 2011. The structure,
785 composition, and dimensions of TiO2 and ZnO nanomaterials in commercial
786 sunscreens. J. Nanoparticle Res. 13, 3607–3617. https://doi.org/10.1007/s11051-
787 011-0438-4
788 Li, M., Lin, D., Zhu, L., 2013. Effects of water chemistry on the dissolution of ZnO
789 nanoparticles and their toxicity to *Escherichia coli*. Environ. Pollut. 173, 97–102.
790 https://doi.org/10.1016/j.envpol.2012.10.026
791 Liu, H., Stephens, T.G., González-Pech, R.A., Beltran, V.H., Lapeyre, B., Bongaerts, P., Cooke,
792 I., Aranda, M., Bourne, D.G., Forêt, S., Miller, D.J., van Oppen, M.J.H., Voolstra, C.R.,
793 Ragan, M.A., Chan, C.X., 2018. Symbiodinium genomes reveal adaptive evolution of
794 functions related to coral-dinoflagellate symbiosis. Commun. Biol. 1, 1–11.
795 https://doi.org/10.1038/s42003-018-0098-3
796 Lopes, S., Ribeiro, F., Wojnarowicz, J., Łojkowski, W., Jurkschat, K., Crossley, A., Soares,
797 A.M.V.M., Loureiro, S., 2014. Zinc oxide nanoparticles toxicity to Daphnia magna:
798 size-dependent effects and dissolution. Environ. Toxicol. Chem. 33, 190–198.
799 https://doi.org/10.1002/etc.2413
800 Lu, Y., Jiang, J., Zhao, H., Han, X., Xiang, Y., Zhou, W., 2020. Clade-Specific Sterol Metabolites
801 in Dinoflagellate Endosymbionts Are Associated with Coral Bleaching in Response to
802 Environmental Cues. mSystems 5, 10.1128/msystems.00765-20.
803 https://doi.org/10.1128/msystems.00765-20
804 Mahalakshmi, S., Hema, N., Vijaya, P.P., 2020. In Vitro Biocompatibility and Antimicrobial
805 activities of Zinc Oxide Nanoparticles (ZnO NPs) Prepared by Chemical and Green
806 Synthetic Route— A Comparative Study. BioNanoScience 10, 112–121.
807 https://doi.org/10.1007/s12668-019-00698-w
808 Manzo, S., Miglietta, M.L., Rametta, G., Buono, S., Di Francia, G., 2013. Toxic effects of ZnO
809 nanoparticles towards marine algae *Dunaliella tertiolecta*. Sci. Total Environ. 445–
810 446, 371–376. https://doi.org/10.1016/j.scitotenv.2012.12.051
811 Marcellin-Gros, R., Piganeau, G., Stien, D., 2020. Metabolomic Insights into Marine
812 Phytoplankton Diversity. Mar. Drugs 18, 78. https://doi.org/10.3390/md18020078
813 Mbanga, O., Cukrowska, E., Gulumian, M., 2022. Dissolution of titanium dioxide
814 nanoparticles in synthetic biological and environmental media to predict their
815 biodurability and persistence. Toxicol. In Vitro 84, 105457.
816 https://doi.org/10.1016/j.tiv.2022.105457

McDougall, K., Gibb, S., Boyd, K., Brown, B., 2006. Chlorophyll-like compounds as novel biomarkers of stress in corals. Mar. Ecol. Prog. Ser. 325, 137–144. https://doi.org/10.3354/meps325137

Miller, I.B., Moeller, M., Kellermann, M.Y., Nietzer, S., Di Mauro, V., Kamyab, E., Pawlowski, S., Petersen-Thiery, M., Schupp, P.J., 2022. Towards the Development of Standardized Bioassays for Corals: Acute Toxicity of the UV Filter Benzophenone-3 to Scleractinian Coral Larvae. Toxics 10, 244. https://doi.org/10.3390/toxics10050244

Mitjans, M., Marics, L., Bilbao, M., Maddaleno, A.S., Piñero, J.J., Vinardell, M.P., 2023. Size Matters? A Comprehensive In Vitro Study of the Impact of Particle Size on the Toxicity of ZnO. Nanomaterials 13, 1800. https://doi.org/10.3390/nano13111800

Nielsen, D.A., Petrou, K., Gates, R.D., 2018. Coral bleaching from a single cell perspective. ISME J. 12, 1558–1567. https://doi.org/10.1038/s41396-018-0080-6

Pagnout, C., Jomini, S., Dadhwal, M., Caillet, C., Thomas, F., Bauda, P., 2012. Role of electrostatic interactions in the toxicity of titanium dioxide nanoparticles toward Escherichia coli. Colloids Surf. B Biointerfaces 92, 315–321. https://doi.org/10.1016/j.colsurfb.2011.12.012

Palacios, O.A., Gomez-Anduro, G., Bashan, Y., de-Bashan, L.E., 2016. Tryptophan, thiamine and indole-3-acetic acid exchange between Chlorella sorokiniana and the plant growth-promoting bacterium Azospirillum brasilense. FEMS Microbiol. Ecol. 92, fiw077. https://doi.org/10.1093/femsec/fiw077

Pei, J., Chen, S., Yu, K., Hu, J., Wang, Y., Zhang, J., Qin, Z., Zhang, R., Kuo, T.-H., Chung, H.-H., Hsu, C.-C., 2022. Metabolomics Characterization of Scleractinia Corals with Different Life-History Strategies: A Case Study about Pocillopora meandrina and Seriatopora hystrix in the South China Sea. Metabolites 12, 1079. https://doi.org/10.3390/metabo12111079

Praveen, P., Viruthagiri, G., Mugundan, S., Shanmugam, N., 2014. Structural, optical and morphological analyses of pristine titanium di-oxide nanoparticles – Synthesized via sol–gel route. Spectrochim. Acta. A. Mol. Biomol. Spectrosc. 117, 622–629. https://doi.org/10.1016/j.saa.2013.09.037

Ramsby, B.D., Shirur, K.P., Iglesias-Prieto, R., Goulet, T.L., 2014. Symbiodinium Photosynthesis in Caribbean Octocorals. PLOS ONE 9, e106419. https://doi.org/10.1371/journal.pone.0106419

Reddy, M.M., Goossens, C., Zhou, Y., Chaib, S., Raviglione, D., Nicolè, F., Hume, B.C.C., Forcioli, D., Agostini, S., Boissin, E., Boss, E., Bowler, C., de Vargas, C., Douville, E., Flores, M., Furla, P., Galand, P.E., Gilson, E., Lombard, F., Pesant, S., Reynaud, S., Sullivan, M.B., Sunagawa, S., Troublé, R., Thurber, R.V., Wincker, P., Zoccola, D., Voolstra, C.R., Allemand, D., Planes, S., Thomas, O.P., Banaigs, B., 2023. Multi-omics determination of metabolome diversity in natural coral populations in the Pacific Ocean. Commun. Earth Environ. 4, 1–10. https://doi.org/10.1038/s43247-023-00942-y

Reichelt-Brushett, A.J., McOrist, G., 2003. Trace metals in the living and nonliving components of scleractinian corals. Mar. Pollut. Bull. 46, 1573–1582. https://doi.org/10.1016/S0025-326X(03)00323-0

Roach, T.N.F., Dilworth, J., H., C.M., Jones, A.D., Quinn, R.A., Drury, C., 2021. Metabolomic signatures of coral bleaching history. Nat. Ecol. Evol. 5, 495–503. https://doi.org/10.1038/s41559-020-01388-7

Rosset, S., Koster, G., Brandsma, J., Hunt, A.N., Postle, A.D., D'Angelo, C., 2019. Lipidome analysis of Symbiodiniaceae reveals possible mechanisms of heat stress tolerance in

reef coral symbionts. Coral Reefs 38, 1241–1253. https://doi.org/10.1007/s00338-019-01865-x
Sakata, K., Yamamoto, K., Ishikawa, H., Yagi, A., Etoh, H., Ina, K., 1990. Chlorophyllone-a, a new pheophorbide-a related compound isolated from ruditapes philippinarum ruditapes philippinarum as an antioxidative compound. Tetrahedron Lett. 31, 1165–1168. https://doi.org/10.1016/S0040-4039(00)88754-7
Samei, M., Sarrafzadeh, M.-H., Faramarzi, M.A., 2019. The impact of morphology and size of zinc oxide nanoparticles on its toxicity to the freshwater microalga, Raphidocelis subcapitata. Environ. Sci. Pollut. Res. 26, 2409–2420. https://doi.org/10.1007/s11356-018-3787-z
Sánchez-Quiles, D., Tovar-Sánchez, A., 2015. Are sunscreens a new environmental risk associated with coastal tourism? Environ. Int. 83, 158–170. https://doi.org/10.1016/j.envint.2015.06.007
Savić, M.P., Sakač, M.N., Kuzminac, I.Z., Ajduković, J.J., 2022. Structural diversity of bioactive steroid compounds isolated from soft corals in the period 2015–2020. J. Steroid Biochem. Mol. Biol. 218, 106061. https://doi.org/10.1016/j.jsbmb.2022.106061
Scheufen, T., Iglesias-Prieto, R., Enríquez, S., 2017. Changes in the Number of Symbionts and Symbiodinium Cell Pigmentation Modulate Differentially Coral Light Absorption and Photosynthetic Performance. Front. Mar. Sci. 4. https://doi.org/10.3389/fmars.2017.00309
Schneider, S.L., Lim, H.W., 2019. A review of inorganic UV filters zinc oxide and titanium dioxide. Photodermatol. Photoimmunol. Photomed. 35, 442–446. https://doi.org/10.1111/phpp.12439
Sikorskaya, T.V., Ermolenko, E.V., Imbs, A.B., 2020. Effect of experimental thermal stress on lipidomes of the soft coral *Sinularia* sp. and its symbiotic dinoflagellates. J. Exp. Mar. Biol. Ecol. 524, 151295. https://doi.org/10.1016/j.jembe.2019.151295
Slomberg, D.L., Catalano, R., Bartolomei, V., Labille, J., 2021. Release and fate of nanoparticulate TiO2 UV filters from sunscreen: Effects of particle coating and formulation type. Environ. Pollut. 271, 116263. https://doi.org/10.1016/j.envpol.2020.116263
Smijs, T.G., Pavel, S., 2011. Titanium dioxide and zinc oxide nanoparticles in sunscreens: focus on their safety and effectiveness. Nanotechnol. Sci. Appl. 4, 95–112. https://doi.org/10.2147/NSA.S19419
Sogin, E.M., Putnam, H.M., Anderson, P.E., Gates, R.D., 2016. Metabolomic signatures of increases in temperature and ocean acidification from the reef-building coral, Pocillopora damicornis. Metabolomics 12, 71. https://doi.org/10.1007/s11306-016-0987-8
Stien, D., Clergeaud, F., Rodrigues, A.M.S., Lebaron, K., Pillot, R., Romans, P., Fagervold, S., Lebaron, P., 2019. Metabolomics Reveal That Octocrylene Accumulates in Pocillopora damicornis Tissues as Fatty Acid Conjugates and Triggers Coral Cell Mitochondrial Dysfunction. Anal. Chem. 91, 990–995. https://doi.org/10.1021/acs.analchem.8b04187
Stien, D., Suzuki, M., Rodrigues, A.M.S., Yvin, M., Clergeaud, F., Thorel, E., Lebaron, P., 2020. A unique approach to monitor stress in coral exposed to emerging pollutants. Sci. Rep. 10, 9601. https://doi.org/10.1038/s41598-020-66117-3
Strohecker, J., Golladay, J., Paramo, Makena, Paramo, Meagan, Rahmany, W.E., Blackstone, N.W., 2021. Reactive Oxygen Species and the Stress Response in Octocorals. Physiol. Biochem. Zool. https://doi.org/10.1086/716857

Suggett, D.J., Smith, D.J., 2020. Coral bleaching patterns are the outcome of complex biological and environmental networking. Glob. Change Biol. 26, 68–79. https://doi.org/10.1111/gcb.14871

Suzuki, T., Casareto, B.E., Shioi, Y., Ishikawa, Y., Suzuki, Y., 2015. Finding of 132, 173-cyclopheophorbide a enol as a degradation product of chlorophyll in shrunk zooxanthellae of the coral Montipora digitata. J. Phycol. 51, 37–45. https://doi.org/10.1111/jpy.12253

T. Botana, M., Chaves-Filho, A.B., Inague, A., Z. Güth, A., Saldanha-Corrêa, F., Müller, M.N., Sumida, P.Y.G., Miyamoto, S., Kellermann, M.Y., Valentine, R.C., Yoshinaga, M.Y., 2022. Thermal plasticity of coral reef symbionts is linked to major alterations in their lipidome composition. Limnol. Oceanogr. 67, 1456–1469. https://doi.org/10.1002/lno.12094

Tang, C.-H., Fang, L.-S., Fan, T.-Y., Wang, L.-H., Lin, C.-Y., Lee, S.-H., Wang, W.-H., 2014a. Cellular membrane accommodation to thermal oscillations in the coral Seriatopora caliendrum. PloS One 9, e105345. https://doi.org/10.1371/journal.pone.0105345

Tang, C.-H., Lin, C.-Y., Lee, S.-H., Wang, W.-H., 2014b. Cellular membrane accommodation of copper-induced oxidative conditions in the coral *Seriatopora caliendrum*. Aquat. Toxicol. 148, 1–8. https://doi.org/10.1016/j.aquatox.2013.12.027

Tang, C.-H., Lin, C.-Y., Lee, S.-H., Wang, W.-H., 2017. Membrane lipid profiles of coral responded to zinc oxide nanoparticle-induced perturbations on the cellular membrane. Aquat. Toxicol. 187, 72–81. https://doi.org/10.1016/j.aquatox.2017.03.021

Thallinger, D., Labille, J., Milinkovitch, T., Boudenne, J.-L., Loosli, F., Slomberg, D., Angeletti, B., Lefrançois, C., 2023. UV filter occurrence in beach water of the Mediterranean coast – A field survey over 2 years in Palavas-les-Flots, France. Int. J. Cosmet. Sci. 45, 67–83. https://doi.org/10.1111/ics.12904

Thorel, E., Clergeaud, F., Rodrigues, A.M.S., Lebaron, P., Stien, D., 2022. A Comparative Metabolomics Approach Demonstrates That Octocrylene Accumulates in Stylophora pistillata Tissues as Derivatives and That Octocrylene Exposure Induces Mitochondrial Dysfunction and Cell Senescence. Chem. Res. Toxicol. 35, 2160–2167. https://doi.org/10.1021/acs.chemrestox.2c00248

Tovar-Sánchez, A., Sánchez-Quiles, D., Basterretxea, G., Benedé, J.L., Chisvert, A., Salvador, A., Moreno-Garrido, I., Blasco, J., 2013. Sunscreen Products as Emerging Pollutants to Coastal Waters. PLOS ONE 8, e65451. https://doi.org/10.1371/journal.pone.0065451

Tsui, M.M.P., Lam, J.C.W., Ng, T.Y., Ang, P.O., Murphy, M.B., Lam, P.K.S., 2017. Occurrence, Distribution, and Fate of Organic UV Filters in Coral Communities. Environ. Sci. Technol. 51, 4182–4190. https://doi.org/10.1021/acs.est.6b05211

Venn, A.A., Wilson, M.A., Trapido-Rosenthal, H.G., Keely, B.J., Douglas, A.E., 2006. The impact of coral bleaching on the pigment profile of the symbiotic alga, Symbiodinium. Plant Cell Environ. 29, 2133–2142. https://doi.org/10.1111/j.1365-3040.2006.001587.x

Vicente, A., Sohm, B., Flayac, J., Rousselle, P., Bauda, P., Pagnout, C., 2018. Toxicity mechanisms of ZnO UV-filters used in sunscreens toward the model cyanobacteria Synechococcus elongatus PCC 7942. Environ. Sci. Pollut. Res. 12, 1669–1677. https://doi.org/10.1007/s11356-019-05057-6

Wang, M., Carver, J.J., Phelan, V.V., Sanchez, L.M., Garg, N., Peng, Y., Nguyen, D.D., Watrous, J., Kapono, C.A., Luzzatto-Knaan, T., Porto, C., Bouslimani, A., Melnik, A. V., Meehan, M.J., Liu, W.-T., Crüsemann, M., Boudreau, P.D., Esquenazi, E., Sandoval-Calderón, M., Kersten, R.D., Pace, L.A., Quinn, R.A., Duncan, K.R., Hsu, C.- C., Floros, D.J.,

Gavilan, R.G., Kleigrewe, K., Northen, T., Dutton, R.J., Parrot, D., Carlson, E.E., Aigle, B., Michelsen, C.F., Jelsbak, L., Sohlenkamp, C., Pevzner, P., Edlund, A., McLean, J., Piel, J., Murphy, B.T., Gerwick, L., Liaw, C.-C., Yang, Y.-L., Humpf, H.-U., Maansson, M., Keyzers, R.A., Sims, A.C., Johnson, A.R., Sidebottom, A.M., Sedio, B.E., Klitgaard, A., Larson, C.B., Boya, P, Torres- Mendoza, D., Gonzalez, D.J., Silva, D.B., Marques, L.M., Demarque, D.P., Pociute, E., O'Neill, E.C., Briand, E., Helfrich, E.J.N., Granatosky, E.A., Glukhov, E., Ryffel, F., Houson, H., Mohimani, H., Kharbush, J.J., Zeng, Y., Vorholt, J.A., Kurita, K.L., Charusanti, P., McPhail, K.L., Nielsen, K.F., Vuong, L., Elfeki, M., Traxler, M.F., Engene, N., Koyama, N., Vining, O.B., Baric, R., Silva, R.R., Mascuch, S.J., Tomasi, S., Jenkins, S., Macherla, V., Hoffman, T., Agarwal, V., Williams, P.G., Dai, J., Neupane, R., Gurr, J., Rodríguez, A.M.C., Lamsa, A., Zhang, C., Dorrestein, K., Duggan, B.M., Almaliti, J., Allard, P.-M., Phapale, P., Nothias, L.-F., Alexandrov, T., Litaudon, M., Wolfender, J.-L., Kyle, J.E., Metz, T.O., Peryea, T., Nguyen, D.-T., VanLeer, D., Shinn, P., Jadhav, A., Müller, R., Waters, K.M., Shi, W., Liu, X., Zhang, L., Knight, R., Jensen, P.R., Palsson, B.Ø., Pogliano, K., Linington, R. G., Gutiérrez, M., Lopes, N.P., Gerwick, W.H., Moore, B.S., Dorrestein, P.C., Bandeira, N., 2016. Sharing and community curation of mass spectrometry data with Global Natural Products Social Molecular Networking. Nat. Biotechnol. 34, 828–837. https://doi.org/10.1038/nbt.3597.

Williams, J., Pettorelli, N., Hartmann, A.C., Quinn, R.A., Plaisance, L., O'Mahoney, M., Meyer, C.P., Fabricius, K.E., Knowlton, N., Ransome, E., 2024. Decline of a distinct coral reef holobiont community under ocean acidification. Microbiome 12, 75. https://doi.org/10.1186/s40168-023-01683-y

Wu, F., Harper, B.J., Harper, S.L., 2019. Comparative dissolution, uptake, and toxicity of zinc oxide particles in individual aquatic species and mixed populations. Environ. Toxicol. Chem. 38, 591–602. https://doi.org/10.1002/etc.4349

Xia, B., Chen, B., Sun, X., Qu, K., Ma, F., Du, M., 2015. Interaction of TiO2 nanoparticles with the marine microalga Nitzschia closterium: growth inhibition, oxidative stress and internalization. Sci. Total Environ. 508, 525–533. https://doi.org/10.1016/j.scitotenv.2014.11.066

Xiong, D., Fang, T., Yu, L., Sima, X., Zhu, W., 2011. Effects of nano-scale TiO2, ZnO and their bulk counterparts on zebrafish: acute toxicity, oxidative stress and oxidative damage. Sci. Total Environ. 409, 1444–1452. https://doi.org/10.1016/j.scitotenv.2011.01.015

Xiong, G., Pal, U., Serrano, J.G., Ucer, K.B., Williams, R.T., 2006. Photoluminesence and FTIR study of ZnO nanoparticles: the impurity and defect perspective. Phys. Status Solidi C 3, 3577–3581. https://doi.org/10.1002/pssc.200672164

Yang, F., Wei, Z., Long, C., Long, L., 2023. Toxicological effects of oxybenzone on the growth and bacterial composition of Symbiodiniaceae. Environ. Pollut. Barking Essex 1987 317, 120807. https://doi.org/10.1016/j.envpol.2022.120807

Yuan, S., Huang, J., Qian, W., Zhu, X., Wang, S., Jiang, X., 2023. Are Physical Sunscreens Safe for Marine Life? A Study on a Coral–Zooxanthellae Symbiotic System. Environ. Sci. Technol. 57, 15846–15857. https://doi.org/10.1021/acs.est.3c04603

Yung, M.M.N., Fougères, P.-A., Leung, Y.H., Liu, F., Djurišić, A.B., Giesy, J.P., Leung, K.M.Y., 2017. Physicochemical characteristics and toxicity of surface-modified zinc oxide nanoparticles to freshwater and marine microalgae. Sci. Rep. 7, 15909. https://doi.org/10.1038/s41598-017-15988-0

Zhou, Z., Ni, X., Wu, Z., Tang, J., 2022. Physiological and transcriptomic analyses reveal the threat of herbicides glufosinate and glyphosate to the scleractinian coral *Pocillopora damicornis*. Ecotoxicol. Environ. Saf. 229, 113074. https://doi.org/10.1016/j.ecoenv.2021.113074

Zovko Končić, M., Ioannou, E., Sawadogo, W.R., Abdel-Razik, A.F., Vagias, C., Diederich, M., Roussis, V., 2016. 4α-Methylated steroids with cytotoxic activity from the soft coral *Litophyton mollis*. Steroids 115, 130–135. https://doi.org/10.1016/j.steroids.2016.08.017